Compensation of Kerr Nonlinearities in Fiber Communication Systems Based on Volterra Theory

Compensation of Kerr Nonlinearities in Fiber Communication Systems Based on Volterra Theory

By

Ling Liu

B.E, Electronics and Information Engineering Dept, Huazhong University of Science and Technology

A Thesis

Submitted to the School of Graduate Studies

in Partial Fulfilment of the Requirements

for the Degree

Masters in Applied Science

McMaster University

by Ling Liu, July, 2006

Masters in Applied Science(2006) McMaster University
Electrical and Computer Engineering Hamilton, Ontario

TITLE: Compensation of Kerr Nonlinearities in Fiber Communication Systems Based on Volterra Theory

AUTHOR: Ling Liu, B. E. (Huazhong University of Science and Technology)
SUPERVISOR: Dr. Shiva Kumar

NUMBER OF PAGES: x, 65

Abstract

This thesis studies the optical and electronic compensation for fiber nonlinearities based on the theory of Volterra expression. Signals propagating through optical fibers suffer from both linear and nonlinear distortion. In this thesis, we first construct an approximate inverse of fiber systems based on the theory of pth-order inverse of Volterra expansion. For a fully dispersion compensated fiber system $\mathbf{H}$ with a second-order dispersion profile $\beta_2(z)$ and a total length of L, if the input field is real, we show that the inverse can be approximated by a system $\hat{\mathbf{K}}$ with an inverted seconder-order dispersion profile $-\beta_2(z-L)$, while keeping all the other parameters the same. We then further develop the scheme by adding an optical phase conjugator (OPC) in the middle of the transmission line. More specifically, the inversion of a fully dispersion compensated N-span fiber system $\mathbf{H}$ with a second-order dispersion profile $\beta_2(z)$ and a total length L, is realized using an OPC followed by another N-span system $\hat{\mathbf{K}}$ with an inverted seconder-order dispersion profile $-\beta_2(z-L)$, while keeping all the other parameters the same. In this way the original input optical signals can be recovered exactly. Our analytical and numerical simulation results show that the scheme works well for both single-channel systems and WDM systems.

For electronic compensation techniques, we examine a nonlinear intersymbol interference (ISI) canceler based on Volterra theory, which was proposed first for voiceband data transmission, and apply it to optical fiber systems here, for the first time to our knowledge. The canceler is able to compensate nonlinear ISI caused by the cross product of both precursor and postcursor.

Acknowledgement

I would like to take this opportunity to thank many people who made this thesis possible. First and foremost, I wish to express my appreciation to my supervisor Dr. Kumar. His guidance, encouragement and understanding during my research are highly appreciated and will always be remembered.

Special thanks to my readers, Dr. Huang and Dr. Xu, for their valuable time. Thanks to Cheryl, Helen, Jill and all other Electrical and Computer Engineering administrative staffs for their friendly assistance.

Sincere thanks to my colleagues Xianming Zhu, Pengju Zhang, Dong Yang, Yanping Xi at the Photonics Laboratory, and my roommates Ying Li and Yan Li. Their help and friendship in the past two years have made my master study enjoyable.

I gratefully dedicate this thesis to my parents, Yuanqing Liu and Hui Huang. Thanks for all their love and support.

Contents

List of Figures

List of Abbreviations

OSNR	Optical Signal-to-Noise Ratio
SNR	Signal-to-Noise Ratio
ASE	Amplifier Spontaneous Emission
CD	Chromatic Dispersion
WDM	Wavelength-Division Multiplexing
SBS	Stimulated Brillouin Scattering
SRS	Stimulated Raman Scattering
SPM	Self-Phase Modulation
XPM	Cross-phase Modulation
FWM	Four-wave mixing
MI	Modulation Instability
PMD	Polarization Mode Dispersion
DGD	Differential Group Delay
OPC	Optical Phase Conjugator
DCF	Dispersion-Compensating Fibers
GVD	Group Velocity Dispersion
DSF	Dispersion-shifted Fiber
SMF	Single-mode Fiber
LE	Linear Equalization
DFE	Decision Feedback Equalization
MLSE	Maximum Likelihood Sequence Estimation

Chapter 1

Introduction

1.1 Introduction to the thesis

The demand for cost-effective transmission of large amount of information has hastened the widespread commercial deployment of lightwave systems. The optical fiber offers unrivaled transmission capacity at a cost lower than any other media, it has emerged as the undisputed transmission medium of choice. Optical fiber systems are employed in nearly all area of telecommunications. However, there are four basic impairments in modern optical transmission systems: the amplified spontaneous emission, chromatic dispersion, nonlinear effects, and polarization mode dispersion [1]-[16].

- **Amplified spontaneous emission (ASE)**

  All amplifiers degrade the signal-to-noise ratio (SNR) of the amplified signal because of ASE that add noise to the signal during the amplification. Optical amplifiers are often cascaded to overcome fiber losses in a long-haul lightwave system, and the ASE becomes a critical factor for such systems. There are two reasons for it. First, in a cascaded chain of optical amplifiers, the ASE accumulates over many amplifiers and degrades the optical SNR as the number of amplifiers increases. Second, as the level of the ASE grows, it begins to saturate optical amplifiers and reduce the gain of amplifiers located further down the fiber link. The net result is that the signal level drops further while the ASE level increases [1][2].

- **Chromatic dispersion (CD)**

  Because of the nonzero bandwidth of an optical signal, the dispersion leads to pulse broadening since different spectral components of the signal travels at different group velocities.

- **Nonlinear effects**

  One of the unique characteristic of optical fibers is their relatively low threshold for nonlinear effects. This can be a serious disadvantage in optical communications, especially in wavelength-division multiplexing (WDM) systems, where many closely

spaced channels propagate simultaneously, resulting in high optical intensities in the fiber [1][2][8]. There are two types of nonlinearities in a typical optical fiber system

1. The nonlinearities that arise from scattering, i.e. stimulated Brillouin scattering (SBS) and stimulated Raman scattering (SRS);
2. The nonlinearities that arise from optically induced changes in the refractive index (Kerr nonlinearities), and result either in phase modulation, i.e. self-phase modulation (SPM) and cross-phase modulation (XPM) (the pulse's phase changes caused by the interaction with itself (SPM) or another pulse in a nonlinear medium (XPM)), or in the mixing of several waves and the generation of new frequencies, i.e. four wave mixing (FWM) (a phenomenon that when three wavelengths interact in a nonlinear medium, they give rise to a fourth wavelength).

- **Polarization mode dispersion (PMD)**

  Physically, PMD has its origin in the birefringence that is present in any optical fiber, and it is a big obstacle for high-capacity long-haul optical communication systems [14]-[16]. Small departures from perfect cylindrical symmetry lead to birefringence because of different mode indices associated with the orthogonally polarized components of the fundamental fiber mode. If the input pulse excites both polarization components, it becomes broader as the two components disperse along the fiber because of their different group velocities. In a first order approximation, PMD, that is described by a differential group delay (DGD) between two orthogonal states of polarization (PSPs), causes an undesired output pulse broadening; the frequency dependence of DGD and PSPs produces other distorting effects, considered as higher order PMD effects.

Various optical and electrical compensation schemes have been proposed to mitigate the above effects [1]-[51]. The chromatic compensation and polarization mode compensation have been studied extensively, but less work was done on the compensation for nonlin-

ear effects. In this thesis, we develop optical and electronic compensation schemes that simultaneously compensate for both chromatic dispersion and Kerr nonlinearities. Our approach is base on the theory of Volterra representation of optical fiber systems.

1.2 Introduction to chapters

The thesis is organized as follows:

1. Chapter 1 gives an introduction to the thesis and a general content of each chapter.

2. Chapter 2 introduces the background of the work in the thesis. A literature survey of optical and electronic compensation scheme for fiber communication systems is introduced first. And then the theory of Volterra representation of nonlinear memory systems and its application to optical fiber systems is described. The work in the following three chapters is based on the Volterra theory.

3. Chapter 3 describes an optical compensation scheme based on the theory of pth-order inverse of Volterra expansion. This scheme is able to compensate CD and Kerr effects for single-channel systems.

4. Chapter 4 extends the scheme proposed in Chapter 3 by adding an Optical Phase Conjugator (OPC) in the middle of the fiber span, this scheme is able to compensation CD and Kerr effects for both single-channel system and WDM systems.

5. Chapter 5 shows an example of electronic compensation scheme of optical fiber systems by using the theory of Volterra expansion.

6. Chapter 6 concludes the work in the thesis.

1.3 Contribution

The main contribution of the thesis is as follows:

1. We proposed an optical compensation scheme by using an inverted second-order dispersion profile, while keeping all the other parameters the same. The simulation shows that the compensated system has a higher Q-factor and a wider dynamic range than the uncompensated system with real input signal.

2. We extend the above compensation scheme by adding an Optical Phase Conjugator (OPC) in the middle of the fiber span. And in this way, our scheme can compensate for not only real input signals, i.e. single channel input, but also for complex input signals, i.e. DPSK and WDM input signals.

3. We use nonlinear canceler for the compensation of fiber nonlinearities. The simulation shows that the BER can be reduced by 1dB.

The research work has resulted in the following publications

(i) Optical compensation of fiber nonlinearities based on the theory of pth-order inverse, submitted to Journal of Lightwave Technology.

(ii) Cancelation of nonlinear phase noise using optical phase conjugation and dispersion inversion in optical transmission systems, submitted to Optics Letters.

(iii) Optimization of duty-cycle of RZ signals and filter bandwidths for optically preamplified receivers, Proc. SPIE-Photonics North 2005 or Proceedings of SPIE, Photonics North 5971A-27 (2005).

Chapter 2

Research Background

2.1 Compensation of optical fiber systems

With the advent of optical amplifiers, fiber losses are no longer a major limiting factor for optical communication systems. Modern lightwave systems are often limited by the dispersion and nonlinear effects. Compensations are implemented at the transmitter, at the receiver, or along the fiber link. Depending on the devices that are used, they can be classified as either optical compensation schemes or electronic compensation schemes. In this section, we review the optical and electronic compensation techniques developed to mitigate the degradation of the optical signals.

2.1.1 Optical Compensation schemes

Optical compensators are usually adopted along the fiber link.

2.1.1.1 Optical Chromatic Dispersion Compensation

The chromatic dispersion is because that the phase velocity and group velocity of light propagating in a fiber depend on the frequency of the input light. In an optical fiber, chromatic dispersion can lead to loss of data due to broadening of the light pulse on the receiving end of the transmission. Many optical techniques for dispersion compensation have been demonstrated. They can be classified into three categories: dispersion-compensating fibers, optical filters, and phase-conjugation techniques.

1. The dispersion-compensating fiber (DCF) is a simple and mature technology used in most modern optical transmission systems to compensate for chromatic dispersion [49]. Commercially available DCF can compensate the dispersion of all common transmission fibers with the required accuracy even for very high bit rates and long distances. After the pulse has been broadened by a positive dispersion in a span, it passes through an equal amount of negative dispersion and the original pulse shape is restored before detection. The compensating negative dispersion were added at the beginning of the span, the end of the span, or distributed along the span.

A shortcoming of DCF is that a relatively long length is required to compensate the group velocity dispersion (GVD), and this add considerably to the link loss, especially in the case of long-haul applications [2].

2. Optical filters that compensate chromatic dispersions often take in the form of interferometers and fiber Bragg gratings[2]. An interferometer, which is sensitive to the frequency of the input light, can acts as an optical filter because of its frequency-dependent transmission characteristics. That a fiber Bragg grating is another choice, is because that there is a stop band, the frequency region in which most of the incident light is reflected back. Fiber grating compensators have the disadvantage that the compensated signal is retro-reflected, so that an optical circulator must be employed to separate the input from the output. However, the gratings offer low loss to non-resonant light passing through them, so multiwavelength operation can be obtained by putting several gratings in series down the fiber, each centered on a different wavelength.

3. Optical phase conjugation, in which optical pulses distorted due to dispersion in a first fiber are reshaped by the following OPC and subsequent propagation through a second fiber with similar dispersive characteristics, was first proposed by Yariv et al. [27] in 1979. As can be seen, all the methods of dispersion compensation discussed above require varying amounts of compensation, depending on the length of the span. OPC is unique in that a single component compensates any span, regardless of the length. The disadvantage of OPC is its complexity. And its advantage is that it can be implemented with commercially-available components and that once assembled, it can compensate any span length.

2.1.1.2 Optical Nonlinear Effects Compensation

Nonlinear pulse-to-pulse interaction is one of the main limiting factors in high-bit-rate transmission systems [9]. The nonlinear phase modulation, i.e. self-phase modulation

(SPM) and cross-phase modulation (XPM), is the phenomenon that the fiber nonlinearity shifts the frequencies of the interacting pulses, which, in turn, results in timing jitter and intersymbol interference. Another impairment resulted from the power dependence of the refractive index is four-wave mixing(FWM). If three optical fields with carrier frequencies ω_1, ω_2 and ω_3 copropagate inside the fiber simultaneously, a fourth field whose frequency ω_4 is related to the other frequencies by a relation $\omega_4 = \omega_1 \pm \omega_2 \pm \omega_3$ will be generated. Several frequencies corresponding to different plus and minus sign combinations are possible in principle. In practice, most of these combinations do not build up because of phase mismatch. Frequency combinations of the form $\omega_4 = \omega_1 + \omega_2 - \omega_3$ are often troublesome for multichannel communication systems since they can become nearly phase-matched when channel wavelengths lie close to the zero-dispersion wavelength. The degenerated FWM process for which $\omega_1 = \omega_2$ is often the dominant process and impacts the system performance most [2].

Kerr nonlinearities described above can in principle be canceled using a device with negative n_2 or by mid-span optical phase conjugation (OPC) at alternate repeater sites. The latter has been used only in limited instances because of a fundamental issue: OPC can compensate for Kerr nonlinearities only when the power and dispersion profile are symmetric with respect to the OPC. The requirement of symmetric power profile is obviously unphysical because of periodic amplification, and therefore the only choice was to reduce absorption by using short fiber spans or using distributed amplification. A more severe limitation is met when long dispersive fiber spans are used with relatively higher bit rates and when one attempts to cancel cross phase modulation (XPM). Under these conditions, dispersion effects combined with a lack of symmetric power distribution with respect to the OPC device makes the distortion introduced by Kerr-nonlinearities irreversible.

Pepper and Yariv indicated correction of the Kerr-like phase distortion using OPC [29], and this work was extended by Fisher et al. showing that OPC cancels the effect of both GVD and SPM [32], both for lossless systems. The effect of SPM compensation in fiber transmission has been experimentally confirmed by compensating for pulse-shape

distortion due to large anomalous GVD and SPM [30], [33]. However, SPM compensation by OPC is limited by the asymmetry of the strength of the Kerr effect along the fiber with respect to the OPC position. This is caused by the asymmetric light intensity change along the fiber due to fiber loss and amplifier gain.

The works of [29] and [32] have focused on lossless cases. To reduce the influence of such an intensity change, a method using path-averaged intensity approximation was proposed [37]. Ref. [37] proposed a new method to compensate exactly for both GVD and SPM in a lossy transmission fiber using OPC. The pulse shape is precompensated before OPC by transmission through a fiber with large dispersion. The ratio of the optical Kerr effect and the dispersion was designed to be equal at each positions before and after the OPC. They showed that a DCF with a large normal dispersion is a practical candidate for a compensation fiber. A computer simulation demonstrates effective compensation for waveform distortion in a 40Gb/s intensity-modulated light transmission. In Ref. [39], a novel scheme that compensates both for Kerr nonlinearities and fiber dispersion is demonstrated. The technique realize symmetric power profile by using a compact $LiNbO_3$ phase conjugator combined with Raman amplification.

Besides the method based on OPC, Mecozzi proposed a way of symmetric dispersion compensation in optical links using highly dispersed pulse transmission. Ref. [24] shows analytically that by splitting the dispersion compensation equally between the input and output of the link, complete cancelation of the timing and amplitude jitter can be obtained in systems where the power profile is symmetric about the center. They have shown that complete cancelation of the timing and amplitude jitter can be achieved by symmetric compensation in optical links in cases where a symmetric power profile is present. And they also demonstrate that a significant reduction in nonlinear penalties can also be achieved in practical cases with lumped in-line amplifiers.

2.1.2 Electrical compensation techniques

From the view of signal processing, the impairments of the optical fiber channel can be treated as intersymbol interferences (ISI). The source of intersymbol interference include nonlinearity in the laser transmitter, chromatic dispersion in systems operated at wavelengths other than the dispersion minimum of the fiber, polarization dispersion, bandwidth limitation in the receiver and mode partition fluctuations. Some of these impairments, such as chromatic dispersion, can be compensated optically. Dispersion compensating fiber (DCF) and optical polarization-mode dispersion (PMD) compensators are examples of such optical components. Optical compensation techniques have the advantage of not requiring high-speed IC technology. However, due to a lack of flexibility and the high cost of these solutions, electronic compensation may be a better choice. Compared with optical compensation. Electronic compensation methods have much less dynamic rage but offer low first installed cost and adaptive dispersion compensation. In this section, we review some electrical signal processing techniques, i.e. linear equalization (LE), decision feedback equalization (DFE), maximum likelihood sequence estimation (MLSE), nonlinear cancelation, and electronic transmitter pre-equalization.

2.1.2.1 Linear Equalization

Linear Equalization is the simplest electrical signal processing technique to compensate for linear distortion. A linear equalizer (transversal filter) can be used between the receiver filter and the detector to compensate ISI. An example is the tapped delay line implementation of the equalizer with N taps with tap weights c_i, $i = 1, \cdots, N$. The output and input relationship of the equalizer is given by

$$y(t) = \sum_{i=0}^{N-1} c_i x(t - iT) \tag{2.1}$$

where T is the tap spacing, $x(t)$ is the input signal and $y(t)$ is the output signal. Some performance issues with LE include weight adjustment techniques, the noise enhancement

of the equalizer, and the linearity of the distortion. A detailed discussion can be found in [48]

2.1.2.2 Decision Feedback Equalization

Electrical decision feedback equalizers (DFE) are used for both chromatic dispersion compensation and polarization-mode dispersion in high speed fiber link. The linear equalizer, also known as feed-forward equalizer (FFE) and the decision feedback equalizer (DFE) are the most attractive equalizer structures due to comparative simple operative simple operation principle. Realizations as single chip circuits have been shown for bit rates at 10 Gb/s. The performance limitations of the DFE result from the fact that the signal it creates to cancel the channel ISI is a purely linear combination of previous received bits, therefore it cannot cancel the nonlinear ISI due to Kerr effects. Nonlinear version of DFE exists [19] [20], where the ISI replica can be a nonlinear function of previously received bits. Unfortunately this structure is fundamentally unable to compensate for nonlinearities excited by the bit currently be detected or by future bits (precursor type nonlinear ISI).

2.1.2.3 Maximum Likelihood Sequence Estimation

Maximum Likelihood Sequence Estimation (MLSE) is the optimum detection technique in that it minimizes the error probability for determining bit sequence, given N received signal samples. It can be complex to implement for large N, although it is useful as a bound on performance. MLSE is robust even in the presence of nonlinearity. The nonlinear channel estimator of an MLSE receiver can accurately model nonlinear ISI regardless of whether it is of precursor or postcursor type. It can also provide accurate modeling of ASE or any other non-Gaussian noise probability density function.

2.1.2.4 Electronic Transmitter Pre-equalization

Compensation at the receiver, using techniques such as feed-forward equalization, decision feedback equalization, and maximum likelihood sequence estimation, have been show to be effective in increasing the dispersion tolerance by up to a factor of two. However, the loss of the optical phase information, after direct detection of the intensity modulated signals, limits the amount of ISI distortion that can be effectively compensated. An alternative method, is the use of electronic precompensation, in which the amplitude and the phase waveforms of the transmitted signal are predistorted to achieve compensation of the fiber distortion. Ref. [22] describe how a precompensation transmitter can be implemented using two digital filters controlling a dual-drive Mach-Zehnder modulator (MZM), and propose a filter architecture based on a look-up table and a D/A converter. Simulation results demonstrated that the length of standard single mode fiber (SSMF) over which 10-Gb/s signals could be transmitted with less than 2-dB eye-opening penalties (EOPs) without optical compensation could be in creased by a factor of ten, form 80km to over 800km [21]. And it is claimed that the technique is applicable to a variety source of optical impairments, including chromatic dispersion, intrachannel nonlinear effects, such as self-phase modulation and intrachannel four-wave mixing. intersymbol interference (ISI) in long-haul fiber-optic systems.

2.2 Background Knowledge of Volterra Representation of Optical Fiber Systems

2.2.1 Volterra Representation of Nonlinear Systems

A system can be defined in a mathematical sense as a rule by which an input x is transformed in to an output y. The output and the input usually are functions of an independent variable such as position or time. If they are only functions of time t, the rule can

be expressed as [56]

$$y(t) = \mathbf{H}[x(t)]. \tag{2.2}$$

In 2.2, $\mathbf{H}$ is called an operator because the output function $y(t)$ can be viewed as being produced by an operation on the input function $x(t)$. In this thesis, we only consider time-invariant systems. Thus if $y(t) = \mathbf{H}[x(t)]$, then $y(t+\tau) = \mathbf{H}[x(t+\tau)]$ for any value of τ since the rule by which an input function is transformed into an output time function does not change with time. If a system is linear and time invariant (LTI), then the output $y(t)$ can be expressed as the convolution of the input $x(t)$ with the system unit impulse response $h(t)$

$$y(t) = \int_{-\infty}^{\infty} h(\tau)x(t-\tau)d\tau. \tag{2.3}$$

The system unit impulse response $h(t)$ completely characterizes the LTI system since, once known, the response to any input can be determined from eq. (2.3).

If the system is nonlinear and has no memory, then the graph of $y(t)$ versus $x(t)$ is a curve which can be expressed in a Taylor series under certain restrictions

$$y(t) = \sum_{n=0}^{\infty} c_n x^n(t) \tag{2.4}$$

The extension of eq. (2.4) to nonlinear time-invariant systems with memory is the Volterra series

$$\begin{aligned} y(t) = h_0 &+ \int_{-\infty}^{\infty} h_1(\tau)x(t-\tau_1)d\tau_1 + \int_{-\infty}^{\infty}\int_{-\infty}^{\infty} h_2(\tau_1,\tau_2)x(t-\tau_1)x(t-\tau_2)d\tau_1 d\tau_2 \\ &+ \int_{-\infty}^{\infty}\int_{-\infty}^{\infty}\int_{-\infty}^{\infty} h_3(\tau_1,\tau_2,\tau_3)x(t-\tau_1)x(t-\tau_2)x(t-\tau_3)d\tau_1 d\tau_2 d\tau_3 + \cdots . \end{aligned} \tag{2.5}$$

Another way of expressing eq. (2.5) is

$$y(t) = h_0 + \mathbf{H_1}[x(t)] + \mathbf{H_2}[x(t)] + \cdots \mathbf{H_n}[x(t)] + \cdots \tag{2.6}$$

in which

$$\mathbf{H_n}[x(t)] = \int_{-\infty}^{\infty} \cdots \int_{-\infty}^{\infty} h_n(\tau_1, \cdots, \tau_n)x(t-\tau_1)\cdots x(t-\tau_n)d\tau_1 \cdots d\tau_n, \tag{2.7}$$

In this representation the symbol $\mathbf{H_n}$, which represents the integral, is called an nth-order Volterra operator. The Volterra series as expressed in eq. (2.5) is a functional series. For a given input function $x(t)$, the integration for a particular time t of each term in the series of eq. (2.5) results in a number.

The Volterra series is a power series with memory. This can be seen by changing the input by a gain factor c so that the new input is $cx(t)$. By use of eq. (2.6) and eq. (2.7), the new output is then

$$\begin{aligned} y(t) &= h_0 + \sum_{n=1}^{\infty} \mathbf{H_n}[cx(t)] \\ &= h_0 + \sum_{n=1}^{\infty} c^n \mathbf{H_n}[x(t)] \end{aligned} \tag{2.8}$$

which is a power series in the amplitude factor c. It is a series with memory since the integrals for $\mathbf{H_n}[x(t)]$ given in eq. (2.7) are convolutions.

2.2.2 Theory of Pth-order Inverse

A basic problem of practical importance is the determination of the inverse of a given system, $\mathbf{H}$, which was discussed in Ref. [55]. The pth-order inverse, $\mathbf{K}$, of a system $\mathbf{H}$ is defined as a system for which the Volterra series of the system $\mathbf{Q}$ formed by the tandem connection of $\mathbf{K}$ and $\mathbf{H}$ is

$$\mathbf{Q}[x] == \mathbf{K}[\mathbf{H}(\mathbf{x})] = x + \sum_{n=p+1}^{\infty} \mathbf{Q_n}[x], \tag{2.9}$$

so that the 2nd through the pth-order Volterra operators of $\mathbf{Q}$ are zero.

In order to present the theory of the pth-order post-inverse of a system, we shall derive the Volterra series of two nonlinear systems connected in tandem First. We shall only consider the case in which the two systems do not interact so that there are no loading effects of one system on the other. The relation between the input, $x(t)$, and response, $y(t)$, of the system $\mathbf{H}$ is given by eq. (2.6). The system $\mathbf{K}$ is a pth-order system with the

response $z(t)$ for the input $y(t)$ so that

$$z(t) = \mathbf{K}[y(t)] = \sum_{n=1}^{p} \mathbf{K_n}[y(t)] \tag{2.10}$$

in which $\mathbf{K_n}$ is an nth-order Volterra operator with the kernel $k_n(\tau_1, \cdots, \tau_n)$. The system $\mathbf{Q}$ formed by the tandem connection of the system $\mathbf{H}$ and $\mathbf{K}$ then can be characterized by the Volterra series

$$z(t) = \mathbf{Q}[z(t)] = \sum_{n=1}^{\infty} \mathbf{Q_n}[x(t)] \tag{2.11}$$

in which $\mathbf{Q_n}$ is an nth-order Volterra operator with the kernel $q_n(\tau_1, \cdots, \tau_n)$. We shall determine the operators $\mathbf{Q_n}$ in terms of the operators $\mathbf{H_n}$ and $\mathbf{K_n}$.

To determine the Volterra operators, $\mathbf{Q_n}$, in terms of $\mathbf{H_n}$ and $\mathbf{K_n}$, we first replace $x(t)$ by $cx(t)$ in eq. (2.11), then

$$z(t) = \mathbf{Q}[cx(t)] = \sum_{n=1}^{\infty} c^n \mathbf{Q_n}[x(t)] \tag{2.12}$$

Eq. (2.12) is a power series in c with the coefficient of c^n being $\mathbf{Q_n}[x(t)]$. Another expression for $z(t)$ by $cx(t)$ can be obtained by substituting eq. (2.8) in eq. (2.10), leading to

$$z = \sum_{m=1}^{p} \mathbf{K_m} \left[\sum_{n=1}^{\infty} c^n y_n \right], \tag{2.13}$$

in which

$$y_n(t) = \mathbf{H_n}[x(t)], \tag{2.14}$$

t is dropped for convenience. From the integral representation of the operator $\mathbf{K_m}$, we have

$$\mathbf{K_m}[\sum_{n=1}^{\infty} c^n y_n] = \sum_{n_1=1}^{\infty} \cdots \sum_{n_m=1}^{\infty} c^{n_1} \cdots c^{n_m} \mathbf{K_m}\{y_{n_1}, \cdots, y_{n_m}\} \tag{2.15}$$

in which

$$\begin{aligned} &\mathbf{K_m}\{y_{n_1}, \cdots, y_{n_m}\} \\ &\quad = \int_{-\infty}^{\infty} \cdots \int_{-\infty}^{\infty} k_m(\tau_1, \cdots, \tau_m) y_{n_1}(t - \tau_1) \cdots y_{n_m}(t - \tau_m) d\tau_1 \cdots d\tau_m \end{aligned} \tag{2.16}$$

By substituting eq. (2.15) in eq. (2.13) the desired second power series in c is

$$z = \sum_{m=1}^{p} \sum_{n_1=1}^{\infty} \cdots \sum_{n_m=1}^{\infty} c^{n_1+\cdots+n_m} \mathbf{K_m}\{y_{n_1}, \cdots, y_{n_m}\} \tag{2.17}$$

The Volterra operators $\mathbf{Q_n}$ now can be obtained in terms of $\mathbf{H_n}$ and $\mathbf{K_n}$ by equating like power of c in eq. (2.12) and eq. (2.17).

For $m = 1$

$$\mathbf{Q_1}[x] = \mathbf{K_1}[y_1] = \mathbf{K_1 H_1}[x] \tag{2.18}$$

For $m = 2$

$$\mathbf{Q_2}[x] = \mathbf{K_1}[y_2] + \mathbf{K_2}[y_1] = \mathbf{K_1 H_2}[x] + \mathbf{K_2 H_1}[x] \tag{2.19}$$

For $m = 3$

$$\mathbf{Q_3}[x] = \mathbf{K_1}[y_3] + \mathbf{K_2}\{y_1, y_2\} + \mathbf{K_2}\{y_2, y_1\} + \mathbf{K}[y_1] \tag{2.20}$$

Since a Volterra operator can be considered symmetric with no loss of generality, we can consider the operators $\mathbf{K_n}$ to be symmetric so that

$$\mathbf{K_2}\{y_1, y_2\} = \mathbf{K_2}\{y_2, y_1\} \tag{2.21}$$

Thus eq. 2.20 can be expressed in the form

$$\mathbf{Q_2}[x] = \mathbf{K_1}[y_3] + 2\mathbf{K_2}\{y_1, y_2\} + \mathbf{K_3}[y_1]. \tag{2.22}$$

The relationship holds that

$$2\mathbf{K_2}\{y_1, y_2\} = \mathbf{K_2}[y_1 + y_2] - \mathbf{K_2}[y_1] - \mathbf{K_2}[y_2]. \tag{2.23}$$

Substituting eq. (2.23) into eq. (2.22), $\mathbf{Q_3}[x]$ can be expressed as

$$\mathbf{Q_3}[x] = \mathbf{K_1}[y_3] + \mathbf{K_2}[y_1 + y_2] - \mathbf{K_2}[y_1] - \mathbf{K_2}[y_2] + \mathbf{K_3}[y_1]. \tag{2.24}$$

With the use of eq. (2.14), the expression for $\mathbf{Q_3}$ in operator notation is

$$\mathbf{Q_3} = \mathbf{K_1 H_3} + \mathbf{K_2}[\mathbf{H_1} + \mathbf{H_2}] - \mathbf{K_2 H_1} - \mathbf{K_2 H_2} + \mathbf{K_3 H_1} \tag{2.25}$$

Following the same procedure, we can deduce the expressions for $\mathbf{Q_n}, n > 3$.

The above results will be needed in deriving the pth-order inverse, $\mathbf{K}$.
We shall determine the Volterra operators, $\mathbf{K_n}$, in order that the system $\mathbf{K}$ be a pth-order post-inverse of the system $\mathbf{H}$. This is accomplished by determining the Volterra operators, $\mathbf{K_n}$, so that the tandem system $\mathbf{Q}$ satisfies the conditions given by eq. (2.9). The first condition to be satisfied from eq. (2.9) is

$$\mathbf{Q_1}[x(t)] = x(t). \tag{2.26}$$

It is clear from eq. (2.18) that this condition is satisfied by a linear operator $\mathbf{K_1}$ which is the inverse of the causal linear operator $\mathbf{H_1}$. The requirement thus is that $\mathbf{K_1} = \mathbf{H_1}^{-1}$ or

$$\tilde{K_1}(\omega) = \frac{1}{\tilde{H}(\omega)} \tag{2.27}$$

in which $\tilde{K_1}(\omega)$ and $\tilde{H_1}(\omega)$ are the Fourier transforms of the Volterra kernels, $k_1(t)$ and $h_1(t)$, respectively. The seconde condition that we need to satisfy from eq. (2.9) is that $\mathbf{Q_2}[x(t)] = 0$. Using eq. (2.19), this requires

$$\mathbf{K_2}[y_1] + \mathbf{K_1}[y_2] = \mathbf{K_2}\mathbf{H_1}[x] + \mathbf{K_1}\mathbf{H_2}[x] = 0 \tag{2.28}$$

This will be satisfied for all x only if the operator $\mathbf{K_2}$ satisfies

$$\mathbf{K_2} = -\mathbf{K_1}\mathbf{H_2}\mathbf{H_1}^{-1} = -\mathbf{K_1}\mathbf{H_1}\mathbf{K_1} \tag{2.29}$$

We can proceed in the same manner to determine each of the operators of the system $\mathbf{K}$.

2.2.3 Volterra Series Transfer Function (VSTF) for single-mode fiber

Schrödinger (NLS) wave equation in a reference frame moving at the velocity of the pulse for monochromatic light in a single-mode fiber is given by [1][52]-[54]

$$\frac{\partial A}{\partial z} = -\frac{\alpha}{2}A - j\frac{\beta_2}{2}\frac{\partial^2 A}{\partial t^2} + j\gamma|A|^2 A, \tag{2.30}$$

where $A(t,z)$ is the slowly varying complex envelope of the optical field at time t and position z along the fiber, $\alpha(z)$ is the fiber loss, $\beta_2(z)$ is the second-order dispersion profile, and $\gamma(z)$ is the nonlinear coefficient of the fiber.

The VSTF is obtained in the frequency domain as a relationship between the Fourier transform of the input $\tilde{X}(\omega)$ and the Fourier transform of the output $\tilde{Y}(\omega)$

$$\tilde{Y}(\omega) = \sum_{n=1}^{\infty} \int \cdots \int \tilde{H}_n(\omega_1, \cdots, \omega_n)\tilde{X}(\omega_1)\cdots\tilde{X}(\omega_n)\delta(\omega - \omega_1 - \cdots - \omega_n)d\omega_1 \cdots d\omega_n \quad (2.31)$$

where $\tilde{H}_n(\omega_1, \omega_2, \cdots, \omega_n)$ is the nth-order frequency domain Volterra kernel. Retaining the first three kernels in the VSTF in eq. (2.31), we obtain the input-output relationship of eq. (2.30) as

$$\tilde{A}(\omega,z) = \tilde{H}_1(\omega,z)\tilde{A}(\omega,0) + \iiint \tilde{H}_3(\omega_1,\omega_2,\omega_3)\tilde{A}(\omega_1,0)\tilde{A}^*(\omega_2,0)\tilde{A}(\omega_3,0)\delta(\omega-\omega_1+\omega_2-\omega_3)d\omega_1 d\omega_2 d\omega_3 \quad (2.32)$$

where $\tilde{A}(\omega,z)$ is the Fourier transform of $A(t,z)$, $\tilde{H}_1(\omega,z)$ and $\tilde{H}_3(\omega_1,\omega_2,\omega_3,z)$ are first- and third-order transfer function (Volterra kernels) of an optical fiber of length z, respectively. All the even-order kernels are set to zero due to the absence of even order nonlinearities in an optical fiber. The initial conditions for the kernels are $\tilde{H}_1(\omega,0) = 1$, and $\tilde{H}_n(\omega_1,\cdots,\omega_n,0) = 0$, for $n = 2,3,\cdots$. And we have

$$\tilde{H}_1(\omega,z) = \int h_1(t,z)\exp(-j\omega t)dt, \quad (2.33)$$

$$\tilde{H}_3(\omega_1,\omega_2,\omega_3,z) = \frac{1}{4\pi^2}\iiint h_3(\tau_1,\tau_2,\tau_3,z)e^{-j\omega_1\tau_1+j\omega_2\tau_2-j\omega_3\tau_3}d\tau_1 d\tau_2 d\tau_3. \quad (2.34)$$

Taking the Fourier transform of eq. (2.30)

$$\frac{\partial\tilde{A}(\omega,z)}{\partial z} = \tilde{G}_1(\omega)\tilde{A}(\omega,z) + \iiint \tilde{G}_3(\omega_1,\omega_2,\omega_3)\tilde{A}(\omega_1,z)\tilde{A}^*(\omega_2,z)\tilde{A}(\omega_3,z)d\omega_1 d\omega_2 d\omega_3 \quad (2.35)$$

where the linear dispersion kernel $G_1(\omega) = -\frac{\alpha}{2} + j\frac{\beta_2}{2}\omega^2$ describes the linear effects. The fiber nonlinearity kernel is $G_3(\omega_1, \omega_2, \omega_3) = j\gamma$ describes the third-order fiber nonlinearities. Substituting eq. (2.32) in eq. (2.35), and comparing the first- and third-order terms gives us the differential equations

$$\frac{\partial \tilde{H}_1(\omega, z)}{\partial z} = \tilde{G}_1(\omega)\tilde{H}_1(\omega, z) \tag{2.36}$$

$$\begin{aligned}\frac{\partial \tilde{H}_3(\omega_1, \omega_2, \omega_3, z)}{\partial z} &= \tilde{G}_1(\omega_1 - \omega_2 + \omega_3)\tilde{H}_3(\omega_1, \omega_2, \omega_3, z) \\ &+\tilde{G}_3(\omega_1, \omega_2, \omega_3)\tilde{H}_1(\omega_1, z)\tilde{H}_1^*(\omega_2, z)\tilde{H}_1(\omega_3, z)\end{aligned} \tag{2.37}$$

Solving these differential equations yields

$$\tilde{H}_1(\omega, z) = ce^{\tilde{G}_1(\omega)z} = e^{-\frac{\alpha}{2}+j\beta_2\omega^2} \tag{2.38}$$

For the real fiber system, if the fiber loss is zero, i.e. $\alpha = 0$, and the second-order dispersion is zero, i.e. $\beta_2 = 0$, the linear transfer function should be "1", i.e. $\tilde{H}_1(\omega, z) = 1$, so $c = 1$, and

$$\tilde{H}_1(\omega, z) = e^{\tilde{G}_1(\omega)z} = e^{-\frac{\alpha}{2}+j\beta_2\omega^2} \tag{2.39}$$

Similarly,

$$\begin{aligned}\tilde{H}_3(\omega_1, \omega_2, \omega_3, z) &= \tilde{G}_3(\omega_1, \omega_2, \omega_3)\frac{e^{(\tilde{G}_1(\omega_1)+\tilde{G}_1^*(\omega_2)+\tilde{G}_1(\omega_3))z}}{\tilde{G}_1(\omega_1) + \tilde{G}_1^*(\omega_2) + \tilde{G}_1(\omega_3) - \tilde{G}_1(\omega_1 - \omega_2 + \omega_3)} \\ &\approx j\frac{\gamma}{4\pi^2}e^{-\frac{\alpha z}{2}+j\frac{\beta_2 z}{2}(\omega_1-\omega_2+\omega_3)^2}\frac{1 - e^{-\alpha z - j\beta_2 z(\omega_1-\omega_2)(\omega_3-\omega_2)}}{\alpha + j\beta_2(\omega_1 - \omega_2)(\omega_3 - \omega_2)}.\end{aligned} \tag{2.40}$$

We can include higher-order Volterra kernels to increase the accuracy of the model. The error incurred in ignoring the kernels of order higher than n is proportional to $P^{(n+2)/2}$, where P is the peak power of the optical field [52].

Now we derive the expression for $\tilde{H}_1(\omega)$ and $\tilde{H}_3(\omega_1, \omega_2, \omega_3)$ for multi-span fibers. Suppose $x_0(t)$ is the input optical signal, and $x_i(t)$ is the output after fiber i. Keeping up to the third-order term, we have

$$x_i = \mathbf{H_{1,i}}[x_{i-1}] + \mathbf{H_{3,i}}[x_{i-1}] \tag{2.41}$$

The operator $\mathbf{H}_{1,i}$ and $\mathbf{H}_{3,i}$ are given in frequency domain

$$\mathbf{H}_{1,i}[x] = \tilde{X}(\omega)\tilde{H}_{1,i}(\omega) \tag{2.42}$$

$$\mathbf{H}_{3,i}[x] = \iiint \tilde{H}_{3,i}(\omega_1,\omega_2,\omega_3,z)\tilde{X}(\omega_1)\tilde{X}^*(\omega_2)\tilde{X}(\omega_3)\delta(\omega-\omega_1+\omega_2-\omega_3)d\omega_1 d\omega_2 d\omega_3 \tag{2.43}$$

where

$$\tilde{H}_{1,i}(\omega) = \sqrt{G_i}e^{-\frac{\alpha_i L_i}{2}+j\frac{\beta_{2,i}L_i}{2}\omega^2}, \tag{2.44}$$

$$\tilde{H}_{3,i}(\omega_1,\omega_2,\omega_3) = j\frac{\gamma_i\sqrt{G_i}}{4\pi^2}e^{-\frac{\alpha_i L_i}{2}+j\frac{\beta_{2,i}L_i}{2}(\omega_1-\omega_2+\omega_3)^2}\frac{1-e^{-\alpha_i L_i - j\beta_{2,i}L_i(\omega_1-\omega_2)(\omega_3-\omega_2)}}{\alpha_i+j\beta_{2,i}(\omega_1-\omega_2)(\omega_3-\omega_2)} \tag{2.45}$$

It can be derived from 2.41

$$x_N = \mathbf{H_1}[x_0] + \mathbf{H_3}[x_0] \tag{2.46}$$

where

$$\mathbf{H}_1[x] = \underbrace{\mathbf{H}_{1,N}\mathbf{H}_{1,N-1}\ldots\mathbf{H}_{1,1}}_{N}[x] \tag{2.47}$$

$$\mathbf{H}_3[x] = \sum_{i=1}^{N}\underbrace{\mathbf{H}_{1,N}\mathbf{H}_{1,N-1}\ldots\mathbf{H}_{1,i+1}}_{N-i}\mathbf{H}_{3,i}\underbrace{\tilde{H}_{1,i-1}\mathbf{H}_{1,i-2}\ldots\mathbf{H}_{1,1}}_{i-1}[x] \tag{2.48}$$

From eq. (2.42) eq. (2.43) eq. (2.44) eq. (2.45) eq. (2.47) and eq. (2.48), we have

$$\tilde{H}_1(\omega) = e^{-\frac{1}{2}\sum_{i=1}^{N}(\alpha_i L_i - j\omega^2\beta_{2,i}L_i)}\prod_{i=1}^{N}\sqrt{G_i}, \tag{2.49}$$

$$\tilde{H}_3(\omega_1,\omega_2,\omega_3) = e^{-\frac{1}{2}\sum_{i=1}^{N}(\alpha_i L_i - j(\omega_1-\omega_2+\omega_3)^2\beta_{2,i}L_i)}\prod_{i=1}^{N}\sqrt{G_i}$$

$$\times\sum_{i=1}^{N}j\frac{\gamma_i}{4\pi^2}\frac{1-e^{-\alpha_i L_i - j(\omega_1-\omega_2)(\omega_3-\omega_2)\beta_{2,i}L_i}}{\alpha_i+j(\omega_1-\omega_2)(\omega_3-\omega_2)\beta_{2,i}}e^{-\sum_{k=1}^{i-1}[\alpha_k L_k + j(\omega_1-\omega_2)(\omega_3-\omega_2)\beta_{2,k}L_k]}\prod_{k=1}^{i-1}G_k. \tag{2.50}$$

2.2.4 The pth-order Inverse of Single-mode Fibers

For the 3rd-order inverse of single-mode fiber, the first- and second-order kernels are given by eq. (2.27) and eq. (2.29), and the third-order kernel $\mathbf{K_3}$ can be obtained by setting eq. (2.25) to zero. For a single-mode fiber, we have $\mathbf{H_2}[x] = 0$, so

$$\mathbf{K_1}[x] = \mathbf{H_1}^{-1}[x], \tag{2.51}$$

$$\mathbf{K_2}[x] = 0, \tag{2.52}$$

$$\mathbf{K_3}[x] = -\mathbf{K_1}[\mathbf{H_3}[\mathbf{K_1}[x]]]. \tag{2.53}$$

For a fully dispersion compensated N-span fiber system,

$$\prod_{i=1}^{N} e^{-\alpha_i L_i} G_i = 1, \tag{2.54}$$

$$\sum_{i=1}^{N} \beta_{2,i} L_i = 0, \tag{2.55}$$

So

$$\tilde{H}_1(\omega) = 1, \tag{2.56}$$

$$\tilde{H}_3(\omega_1, \omega_2, \omega_3) = \sum_{i=1}^{N} \{ e^{-\sum_{k=1}^{i-1} [\alpha_k L_k + j(\omega_1 - \omega_2)(\omega_3 - \omega_2)\beta_{2,k} L_k]} \prod_{k=1}^{i-1} G_k \cdot j \frac{\gamma_i}{4\pi^2} \frac{1 - e^{-\alpha_i L_i - j(\omega_1 - \omega_2)(\omega_3 - \omega_2)\beta_{2,i} L_i}}{\alpha_i + j(\omega_1 - \omega_2)(\omega_3 - \omega_2)\beta_{2,i}} \}. \tag{2.57}$$

The pth-order inverse is given by

$$\mathbf{K_1}[x] = x, \tag{2.58}$$

$$\mathbf{K_2}[x] = 0, \tag{2.59}$$

$$\mathbf{K_3}[x] = -\mathbf{H_3}[x]. \tag{2.60}$$

which is

$$\tilde{K}_1(\omega) = 1, \tag{2.61}$$

$$\tilde{K}_3(\omega_1, \omega_2, \omega_3) = -\tilde{H}_3(\omega_1, \omega_2, \omega_3). \tag{2.62}$$

2.3 Conclusion

In this section, we first reviewed optical and electronic compensation techniques for optical fiber systems. Then we introduced the theory of Volterra representation of nonlinear systems with memory, and showed its application to describe single-mode fibers. The designs in the following chapters are based on it.

Chapter 3

Optical Compensation of Fiber Nonlinearities Based on the Theory of Pth-order Inverse

3.1 Introduction

Signals propagating through optical fibers suffer from both linear and nonlinear distortion. The fiber nonlinear effects such as self-phase modulation (SPM), cross-phase modulation (XPM) and four-wave mixing (FWM) are significant factors that limit the performance of optical communication systems. A nonrecursive Volterra series transfer function (VSTF) approach for solving the nonlinear Schrödinger (NLS) wave equation for a single-mode optical fiber is presented in [52][53], and it provides an analytical tool to study the effects of fiber nonlinearities.

In this chapter, we construct an approximate inverse of fiber systems based on the theory of pth-order inverse of Volterra expansion. For a fully dispersion compensated fiber system $\mathbf{H}$ with a second-order dispersion profile $\beta_2(z)$ and a total length of L, if the input field is real, we show that the inverse can be approximated by a system $\hat{\mathbf{K}}$ with an inverted seconder-order dispersion profile $-\beta_2(z-L)$, while keeping all the other parameters the same. Refs. [24][25] have shown that the timing and amplitude jitter due to intrachannel impairments can be suppressed using symmetric dispersion maps, i.e., if L is the midpoint, and $\beta_2(z)$ is the dispersion profile for $0 < z \leq L$, the dispersion profile after the midpoint is $\beta_2(2L-z)$ for $L < z \leq 2L$. We show that such a symmetric dispersion map is a special case of a more general dispersion profile $-\beta_2(z-L)$. The design examples are provided to illustrate the approximate inverse obtained by symmetric as well as non-symmetric dispersion profile.

3.2 Constructing an approximate inverse by inverted second-order dispersion profile

In Chapter 2, we have derived the pth-order inverse for a fully dispersion compensated fiber system. The first- and third-order Volterra kernels are given by eq. (2.61) and eq.

(2.62), where $\tilde{H}_1(\omega)$ and $\tilde{H}_3(\omega_1,\omega_2,\omega_3)$ are given by eq. (2.56) and eq. (2.57). As pointed out in Ref. [52], the inverse transfer function can be obtained by transmitting the optical signal in a fiber system with negative nonlinear coefficient. However, it is hard to find such a material, so we approximate the pth-order inverse $\mathbf{K}$ by another N-span fiber system $\hat{\mathbf{K}}$ with $-\beta_{2,i}$ instead of $\beta_{2,i}$ for each span, while keeping other parameters the same. In this way, we have

$$\hat{\tilde{K}}_1(\omega) = 1, \tag{3.1}$$

$$\hat{\tilde{K}}_3(\omega_1,\omega_2,\omega_3) = -\tilde{H}_3^*(\omega_1,\omega_2,\omega_3) \tag{3.2}$$

We show below that for real input $y(t)$

$$|\mathbf{K}[y]|^2 = |\hat{\mathbf{K}}[y]|^2 \tag{3.3}$$

which means after the photo-detector, $\hat{\mathbf{K}}$ gives exactly the same result as $\mathbf{K}$.
By definition, we have

$$|\mathbf{K}[y]|^2 = |y(t) + \iiint k_3(\tau_1,\tau_2,\tau_3)y(t-\tau_1)y^*(t-\tau_2)y(t-\tau_3)d\tau_1 d\tau_2 d\tau_3|^2, \tag{3.4}$$

where

$$\begin{aligned} k_3(\tau_1,\tau_2,\tau_3) &= \frac{1}{2\pi}\iiint \tilde{K}_3(\omega_1,\omega_2,\omega_3)e^{j\omega_1\tau_1 - j\omega_2\tau_2 + j\omega_3\tau_3}d\omega_1 d\omega_2 d\omega_3 \\ &= -\frac{1}{2\pi}\iiint \tilde{H}_3(\omega_1,\omega_2,\omega_3)e^{j\omega_1\tau_1 - j\omega_2\tau_2 + j\omega_3\tau_3}d\omega_1 d\omega_2 d\omega_3. \end{aligned} \tag{3.5}$$

And

$$|\hat{\mathbf{K}}[y]|^2 = |y(t) + \iiint \hat{k}_3(\tau_1,\tau_2,\tau_3)y(t-\tau_1)y^*(t-\tau_2)y(t-\tau_3)d\tau_1 d\tau_2 d\tau_3|^2 \tag{3.6}$$

(a) exact inverse (b) approximate inverse

Figure 3.1: Comparison of exact inverse and approximate inverse

where

$$\begin{aligned}
\hat{k}_3(\tau_1,\tau_2,\tau_3) &= \frac{1}{2\pi}\iiint \hat{\tilde{K}}_3(\omega_1,\omega_2,\omega_3)e^{j\omega_1\tau_1-j\omega_2\tau_2+j\omega_3\tau_3}d\omega_1 d\omega_2 d\omega_3 \\
&= -\frac{1}{2\pi}\iiint \tilde{H}_3^*(\omega_1,\omega_2,\omega_3)e^{j\omega_1\tau_1-j\omega_2\tau_2+j\omega_3\tau_3}d\omega_1 d\omega_2 d\omega_3 \\
&= -\frac{1}{2\pi}\iiint \tilde{H}_3^*(-\omega_1,-\omega_2,-\omega_3)e^{-j\omega_1\tau_1+j\omega_2\tau_2-j\omega_3\tau_3}d\omega_1 d\omega_2 d\omega_3 \\
&= -\frac{1}{2\pi}\iiint \tilde{H}_3^*(\omega_1,\omega_2,\omega_3)e^{-j\omega_1\tau_1+j\omega_2\tau_2-j\omega_3\tau_3}d\omega_1 d\omega_2 d\omega_3 \\
&= -\frac{1}{2\pi}\left[\iiint \tilde{H}_3(\omega_1,\omega_2,\omega_3)e^{j\omega_1\tau_1-j\omega_2\tau_2+j\omega_3\tau_3}d\omega_1 d\omega_2 d\omega_3\right]^* \\
&= k_3^*(\tau_1,\tau_2,\tau_3)
\end{aligned} \tag{3.7}$$

for real input $y(t)$, we have

$$\hat{\mathbf{K}}[y] = \mathbf{K}[y]^* \tag{3.8}$$

and it follows that

$$|\mathbf{K}[y]|^2 = |\hat{\mathbf{K}}[y]|^2 \tag{3.9}$$

For fiber systems described in Fig. 3.1, if $\mathrm{Re}[y] \gg \mathrm{Im}[y]$, $|\mathbf{K}[y]|^2 \approx |\hat{\mathbf{K}}[y]|^2$, and $|z|^2 \approx |\hat{z}|^2$. The output of the exact inverse $\mathbf{K}$ is z which equals input signal x within the approximation of the 3rd-order Volterra expansion, so $|\hat{z}|^2 \approx |x|^2$, which means that the output power $|\hat{z}|^2$ approximately equals to input power $|x|^2$. Thus the system can be inverted by $\hat{\mathbf{K}}$.

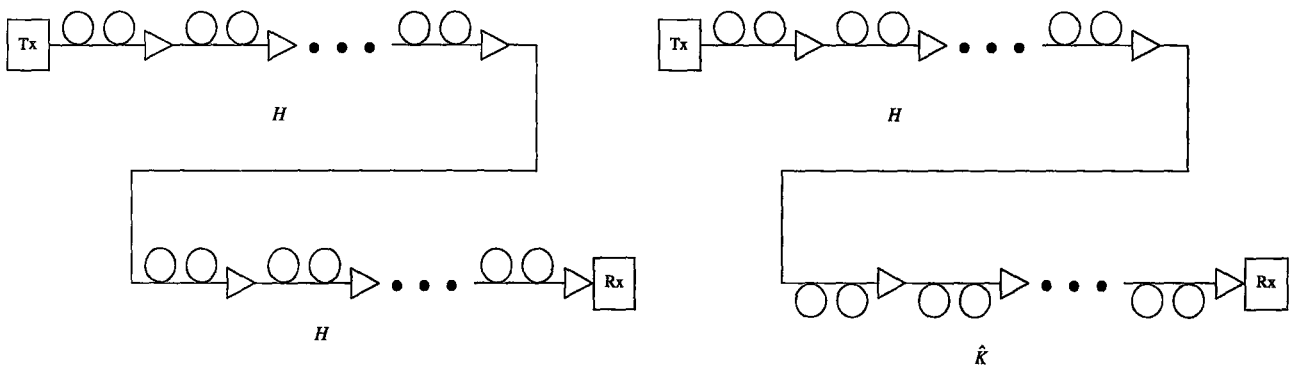

(a) System I (b) System II

Figure 3.2: Fig. 3.2(a) is two identical and fully compensated fiber system **H** connected in tandem. Fig.3.2(b)is the system **H** and its approximate inverse $\hat{\mathbf{K}}$ connected in tandem.

For a fully dispersion compensated fiber system **H** with a second-order dispersion profile $\beta_2(z)$ and a total length of L, if the input field is real, its inverse can be approximated by a system $\hat{\mathbf{K}}$ with an inverted seconder-order dispersion profile $-\beta_2(z-L)$, while keeping all the other parameters the same.

3.3 Design example

We compare system performance of two systems described in Fig. 3.2. Fig. 3.2(a) shows System I which is a tandem connection of two identical and fully dispersion compensated fiber systems **H**. Fig. 3.2(b) shows System II which is a tandem connection of the system **H** and its approximate inverse $\hat{\mathbf{K}}$ described in Section 3.2. Numerical simulations are carried out with the following parameters: bit rate $B = 40$Gb/s, and $\lambda = 1.55\mu$m. The Gaussian pulses with FWHM=8ps are launched to a dispersion managed fiber with nonlinear coefficient $\gamma = 2.7\text{W}^{-1}\text{km}^{-1}$, and fiber loss $\alpha = 0.2$dB/km. The dispersion managed fiber consists of two sections: the first section is a fiber with $D = -7$ps/(nm·km), and of length 40km, followed by a second fiber of the same length with $D = 7$ps/(nm·km).

Amplifier space= 80km, electrical filter is assumed to be ideal low pass filter with a bandwidth of 100GHz. 4096 bits are simulated with a simulation bandwidth of 1280GHz.

3.3.1 Symmetric inverse

Fig. 3.3 show an example of the dispersion profile, which is symmetric with respect to the midpoint. Figs. 3.3(a) and 3.3(b) show the dispersion profile for System I and System II, respectively. Figs. 3.3(c) and 3.3(d) show the eye diagrams of the output from the two systems in the absence of the amplifier noise. Figs. 3.3(e) and 3.3(f) show the eye diagrams of the output from the two systems with noise figure $F = 5.5$dB. From Figs. 3.3(d) and 3.3(f), we see that the eye opening is increased for System II. This is because of the nonlinear compensation provided by the approximate inverse $\hat{\mathbf{K}}$. Fig. 3.4 shows the Q-factor as a function of input power for System I and System II, and the improvement in Q-factor using the inverted dispersion profile $-\beta_2(z-L)$ can be clearly seen. The small fluctuation in Fig. 3.3(d) is due to the factor that the output y of $\mathbf{H}$ has a small imaginary component because of fiber nonlinear effects, and therefore, the inverse provided by $\hat{\mathbf{K}}$ is not exact.

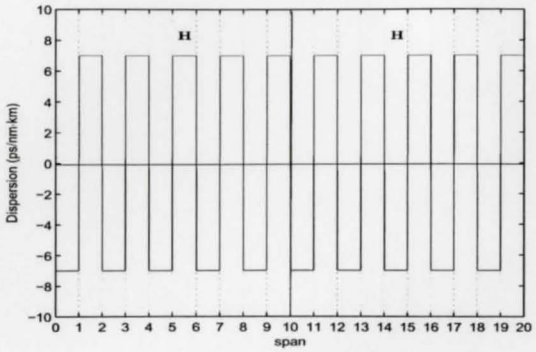

(a) β_2 for System I

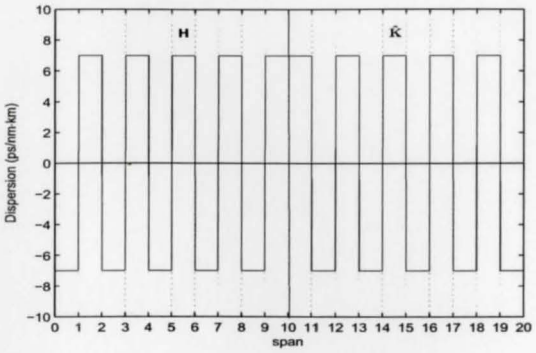

(b) β_2 for System II

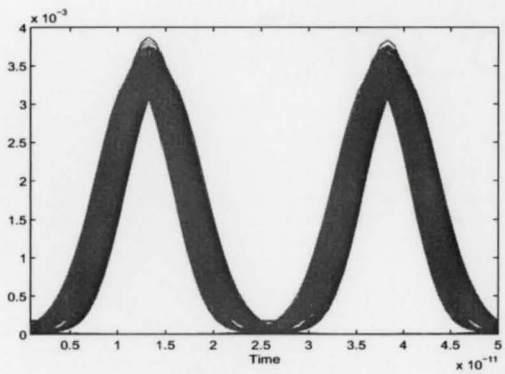

(c) Eye diagram of the output for System I without amplifier noise

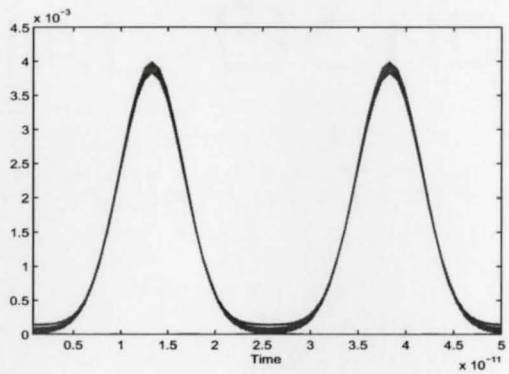

(d) Eye diagram of the output for System II without amplifier noise

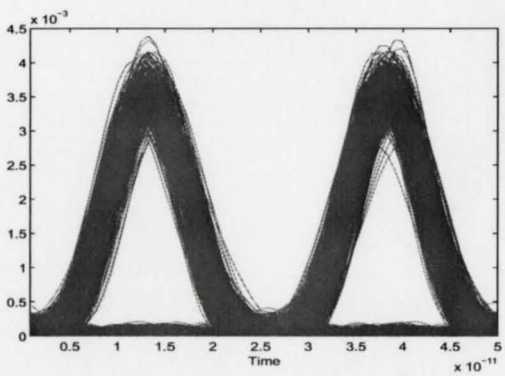

(e) Eye diagram of the output for System I with amplifier noise

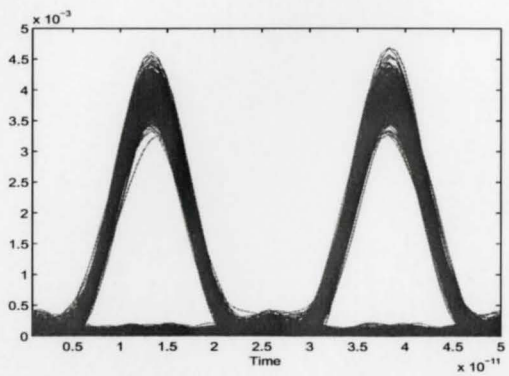

(f) Eye diagram of the output for System II with amplifier noise

Figure 3.3: Eye diagrams of the output signal for a symmetric map.

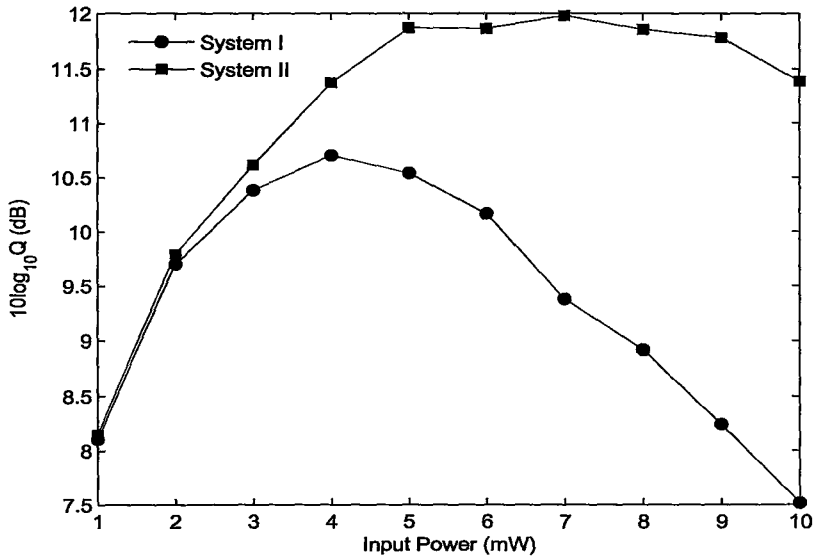

Figure 3.4: Comparison of Q factors of System I and System II for a symmetric map with $F = 5.5$dB

3.3.2 Non-symmetric inverse

Fig. 3.5 shows an example of the dispersion profile, which is non-symmetric with respect to the midpoint. The subsystem $\hat{\mathbf{K}}$ of System II still satisfies the condition $-\beta_2(z-L)$. Figs. 3.5(a) and 3.5(b) show the dispersion profiles for System I and System II, respectively. Figs. 3.5(c) and 3.5(d) show the eye diagrams of the output from the two systems in the absence of amplifier noise. Figs. 3.5(e) and 3.5(f) show the eye diagrams of the output from the two systems with noise figure $F = 5.5$dB. From Figs. 3.5(d) and 3.5(f), we see that the eye opening is increased for System II. This is because of the nonlinear compensation provided by the approximate inverse $\hat{\mathbf{K}}$. The improvement of Q factors is shown in Fig. 3.6.

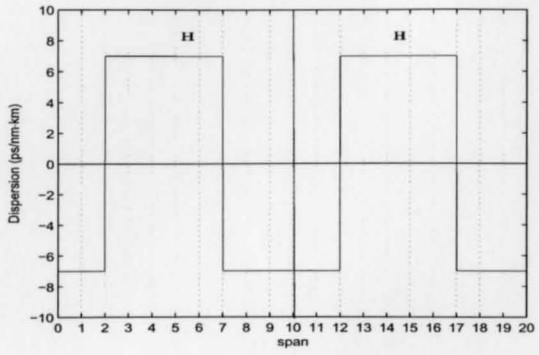

(a) β_2 for System I

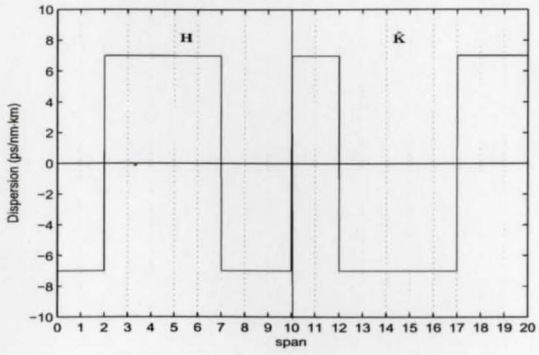

(b) β_2 for System II

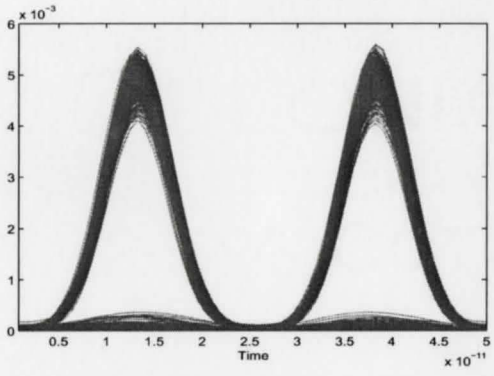

(c) Eye diagram of the output for System I without amplifier noise

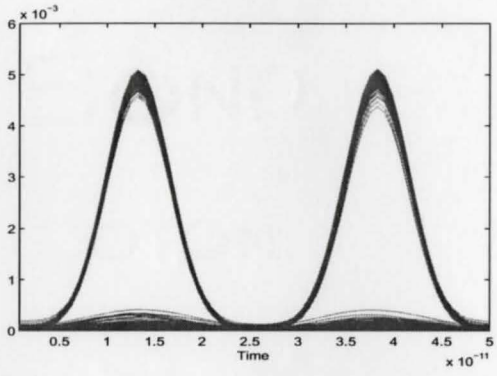

(d) Eye diagram of the output for System II without amplifier noise

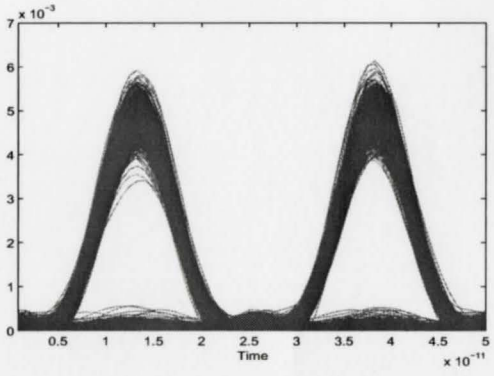

(e) Eye diagram of the output for System I with amplifier noise

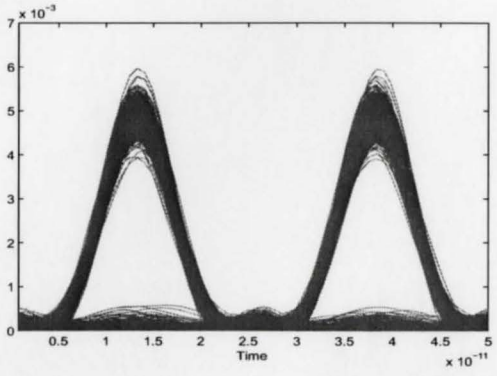

(f) Eye diagram of the output for System II with amplifier noise

Figure 3.5: Eye diagrams of the output signal for a non-symmetric dispersion map.

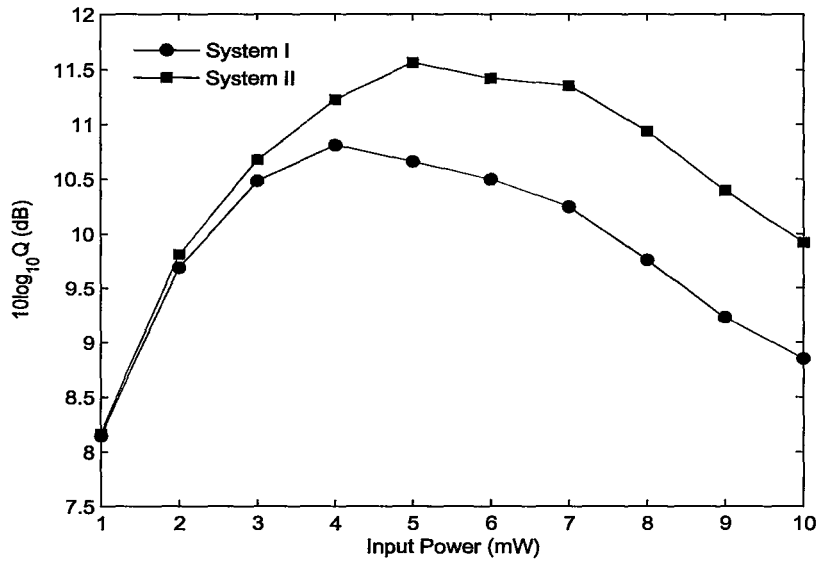

Figure 3.6: Comparison of Q factors of System I and System II for a non-symmetric map with $F = 5.5$dB

3.4 Conclusion

We have proposed an easy way to design the inverse of fiber systems based on the theory of pth-order inverse of Volterra expansion [58]. For a fully dispersion compensated fiber system $\mathbf{H}$ with a second-order dispersion profile $\beta_2(z)$ and a total length of L, the inverse is approximated by a system $\hat{\mathbf{K}}$ with an inverted seconder-order dispersion profile $-\beta_2(z-L)$, while keeping all the other parameters the same. Our simulation shows that the Q factor is improved with our design, especially when fiber nonlinearities are the main source of system noise.

Chapter 4

Construction of the pth-order Inverse of Fiber Transmission Systems Using Optical Phase Conjugation and Inverted Dispersion Profile

4.1 Introduction

Fiber nonlinearities can cause severe impairments in a fiber communication system, and thus limit the transmission capacity of such a system [1] [2]. Various techniques have been proposed to mitigate the Kerr nonlinearities, such as symmetric fiber-link configuration [24][25], optimized precompensation [13], and optical phase conjugation [27][39]. Traditional OPC can undo the effects of seconde-order dispersion and nonlinearities only if the fiber-link is symmetric in dispersion and loss profiles with respect to the location of OPC [2][27]. Although the dispersion profile can be made symmetric with respect to the middle point, it is hard to achieve a symmetric loss profile in practice. Instead, in this chapter, we propose a new scheme that can compensate the Kerr nonlinearities up to the third-order term in Volterra series [52] using OPC and inverted dispersion profile. This is an extension of the scheme proposed in Chapter 3. By adding an OPC in the middle of the span, the original input optical signals can be recovered exactly. More specifically, the inversion of a fully dispersion compensated N-span fiber system $\mathbf{H}$ with a second-order dispersion profile $\beta_2(z)$ and a total length L, is realized using an optical phase conjugator (OPC) followed by another N-span system $\hat{\mathbf{K}}$ with an inverted seconder-order dispersion profile $-\beta_2(z-L)$, while keeping all the other parameters the same. Our analytical and numerical simulation results show that the scheme works well for both single-channel systems and WDM systems.

4.2 Constructing an inverse by an OPC followed by an inverted second-order dispersion profile

In Chapter 2, we have derived the pth-order inverse for a fully dispersion compensated fiber system. The first- and third-order Volterra kernels are given by eq. (2.61) and eq. (2.62), where $\tilde{H}_1(\omega)$ and $\tilde{H}_3(\omega_1,\omega_2,\omega_3)$ are given by eq. (2.56) and eq. (2.57). We

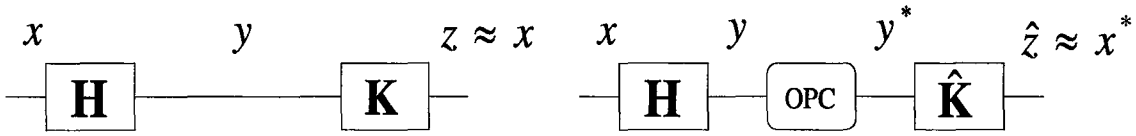

(a) Exact inverse $\mathbf{K}$

(b) Realization of an inverse using an OPC followed by $\hat{\mathbf{K}}$

Figure 4.1: Comparison of the exact inverse and realization of an inverse by an OPC followed by $\hat{\mathbf{K}}$

approximate $\mathbf{K}$ by an OPC followed by another N-span fiber system $\hat{\mathbf{K}}$ with $-\beta_{2,i}$ instead of $\beta_{2,i}$ for each span, while keeping other parameters the same. So

$$\hat{\tilde{K}}_1(\omega) = 1, \tag{4.1}$$

$$\hat{\tilde{K}}_3(\omega_1, \omega_2, \omega_3) = -\tilde{H}_3^*(\omega_1, \omega_2, \omega_3) \tag{4.2}$$

We show below that in Fig. 4.1

$$|\mathbf{K}[y]|^2 = |\hat{\mathbf{K}}[y^*]|^2 \tag{4.3}$$

which means after the photo-detector, $\hat{K}$ gives exactly the same result as K.
By definition, we have

$$|\mathbf{K}[y]|^2 = \left| y(t) + \iiint k_3(\tau_1, \tau_2, \tau_3) y(t-\tau_1) y^*(t-\tau_2) y(t-\tau_3) d\tau_1 d\tau_2 d\tau_3 \right|^2 \tag{4.4}$$

where

$$\begin{aligned} k_3(\tau_1, \tau_2, \tau_3) &= \frac{1}{2\pi} \iiint \tilde{K}_3(\omega_1, \omega_2, \omega_3) e^{j\omega_1\tau_1 - j\omega_2\tau_2 + j\omega_3\tau_3} d\omega_1 d\omega_2 d\omega_3 \\ &= -\frac{1}{2\pi} \iiint \tilde{H}_3(\omega_1, \omega_2, \omega_3) e^{j\omega_1\tau_1 - j\omega_2\tau_2 + j\omega_3\tau_3} d\omega_1 d\omega_2 d\omega_3 \end{aligned} \tag{4.5}$$

And

$$|\hat{\mathbf{K}}[y^*]|^2 = \left| y^*(t) + \iiint \hat{k}_3(\tau_1, \tau_2, \tau_3) y^*(t-\tau_1) y(t-\tau_2) y^*(t-\tau_3) d\tau_1 d\tau_2 d\tau_3 \right|^2 \tag{4.6}$$

where

$$\begin{aligned}
\hat{k}_3(\tau_1,\tau_2,\tau_3) &= \frac{1}{2\pi}\iiint \hat{\tilde{K}}_3(\tau_1,\tau_2,\tau_3)e^{j\omega_1\tau_1-j\omega_2\tau_2+j\omega_3\tau_3}d\omega_1 d\omega_2 d\omega_3 \\
&= -\frac{1}{2\pi}\iiint \tilde{H}_3^*(\omega_1,\omega_2,\omega_3)e^{j\omega_1\tau_1-j\omega_2\tau_2+j\omega_3\tau_3}d\omega_1 d\omega_2 d\omega_3 \\
&= -\frac{1}{2\pi}\iiint \tilde{H}_3^*(-\omega_1,-\omega_2,-\omega_3)e^{-j\omega_1\tau_1+j\omega_2\tau_2-j\omega_3\tau_3}d\omega_1 d\omega_2 d\omega_3 \\
&= -\frac{1}{2\pi}\iiint \tilde{H}_3^*(\omega_1,\omega_2,\omega_3)e^{-j\omega_1\tau_1+j\omega_2\tau_2-j\omega_3\tau_3}d\omega_1 d\omega_2 d\omega_3 \\
&= -\frac{1}{2\pi}\left[\iiint \tilde{H}_3(\omega_1,\omega_2,\omega_3)e^{j\omega_1\tau_1-j\omega_2\tau_2+j\omega_3\tau_3}d\omega_1 d\omega_2 d\omega_3\right]^* \\
&= k_3^*(\tau_1,\tau_2,\tau_3)
\end{aligned} \tag{4.7}$$

for the input $y(t)$, we have

$$\hat{\mathbf{K}}[y] = \mathbf{K}[y^*]^* \tag{4.8}$$

and it follows that

$$|\mathbf{K}[y]|^2 = |\hat{\mathbf{K}}[y^*]|^2 \tag{4.9}$$

Figs. 4.1 show the comparison between the exact inverse $\mathbf{K}$ and an inverse obtained by OPC followed by $\hat{\mathbf{K}}$. If $z(t)$ and $\hat{z}(t)$ are the output of the system with inverse $\mathbf{K}$ (Fig. 4.1(a)) and the system using an OPC followed by $\hat{\mathbf{K}}$ (Fig. 4.1(b)), respectively, it follows that

$$z(t) = \hat{z}^*(t) \tag{4.10}$$

The photo current of a photodetector is proportional to the optical power $|z(t)|^2$, so the system consisting of an OPC and $\hat{\mathbf{K}}$ gives the same result as the system with exact inverse $\mathbf{K}$. So The practical realization of the inverse $\mathbf{K}$ up to the third-order kernel can be done by passing the output of the N-span fiber system $\mathbf{H}$ with dispersion profile $\beta_2(z)$ and total length L through an OPC followed by another N-span fiber system $\hat{\mathbf{K}}$ with an inverted dispersion profile $-\beta_2(z-L)$, while the other parameters of the system $\hat{\mathbf{K}}$ is same as that for $\mathbf{H}$.

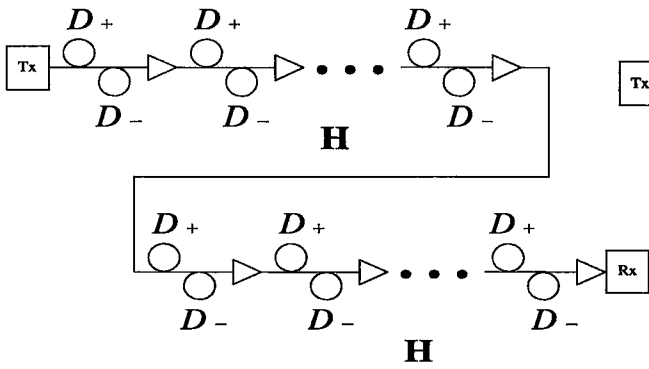

(a) System I: without compensation $\hat{\mathbf{K}}$ and without OPC

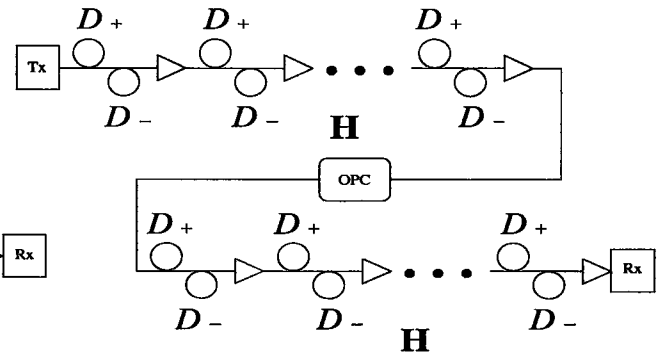

(b) System II: without compensation $\hat{\mathbf{K}}$ and with OPC

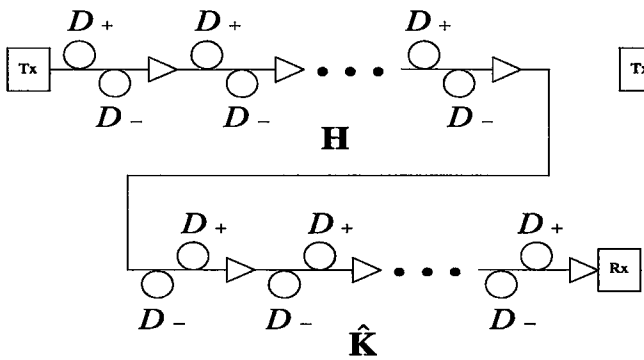

(c) System III: with compensation $\hat{\mathbf{K}}$ and without OPC

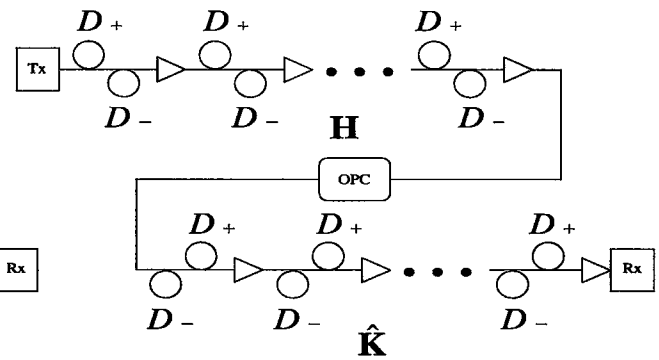

(d) System IV: with compensation $\hat{\mathbf{K}}$ and with OPC. $D_+ = D_-$

Figure 4.2: System description

4.3 Design example

We compare system performance of four systems described in Fig. 4.2. Fig. 4.2(a) shows System I, which is a tandem connection of two identical and fully dispersion compensated fiber systems **H** without mid-span OPC. Fig. 4.2(b) shows System II, which is a tandem connection of two identical and fully dispersion compensated fiber systems **H** with mid-span OPC. Fig. 4.2(c) shows System III, which is a tandem connection of the system **H** and the compensation system $\hat{\mathbf{K}}$ without mid-span OPC. Fig. 4.2(d) shows System IV, which is a tandem connection of the system **H** and the compensation system $\hat{\mathbf{K}}$ with

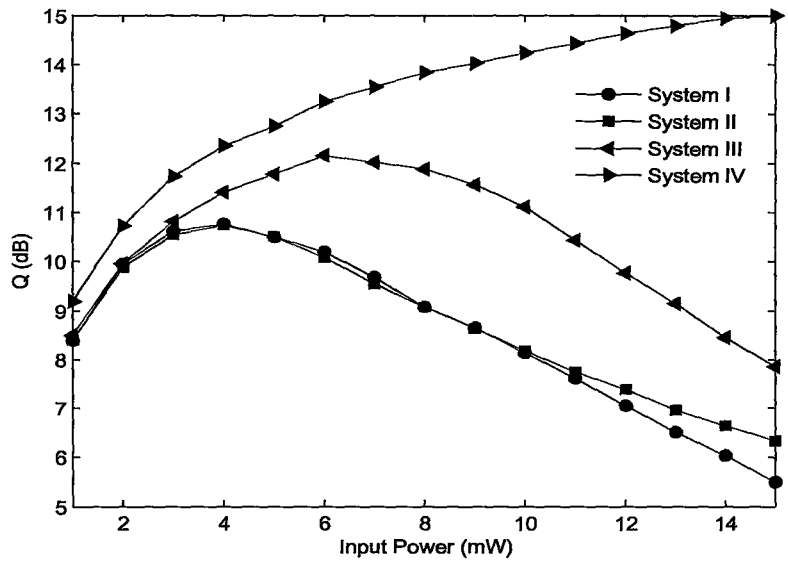

Figure 4.3: Comparison of Q factors of the four fiber Systems for a single channel system

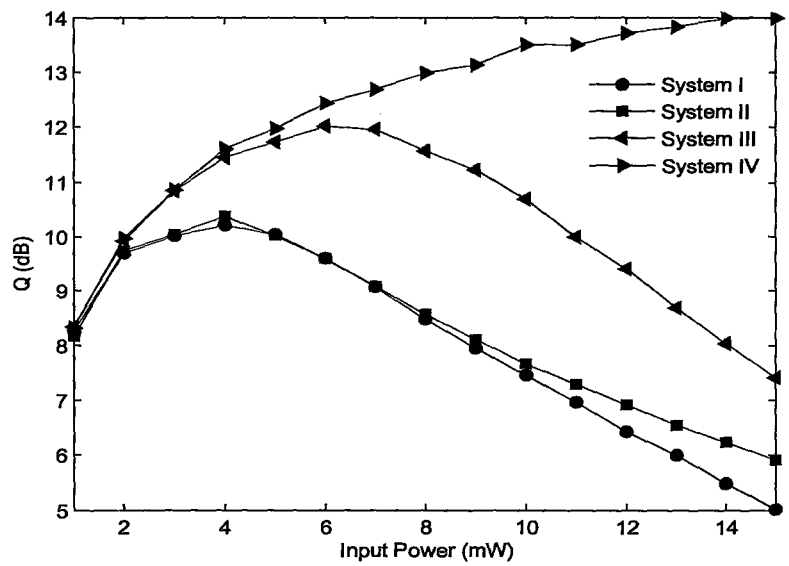

Figure 4.4: Comparison of Q factors of the four fiber systems for the central channel in a WDM system with five channels

mid-span OPC.

We have performed the numerical simulations of Eq. (2.30) with the follow ing parameters: bit rate $B = 40$Gb/s, FWHM=8ps, wavelength $\lambda = 1.55\mu$m, and noise figure $F = 5.5$dB. $\mathbf{H}$ is a 10-span dispersion managed fiber system as shown in Figs. 4.2, with nonlinear coefficient $\gamma = 2.7\text{W}^{-1}\text{km}^{-1}$, dispersion $D = \pm 7\text{ps}/(\text{nm} \cdot \text{km})$, and loss $\alpha = 0.2$dB/km. The dispersion managed fiber consists of two sections: the first section is a fiber with $D_+ = 7\text{ps}/(\text{nm} \cdot \text{km})$, and of length 40km, followed by a second fiber of the same length with $D_- = -7\text{ps}/(\text{nm} \cdot \text{km})$. $\hat{\mathbf{K}}$ is a 10-span fiber system with inverted dispersion profile as shown in Figs. 4.2(c) and 4.2(d). Amplifier spacing= 80km, total transmission distance= 800km, optical filter is assumed to be an ideal bandpass filter with a full bandwidth of 200GHz. 4096 bits are simulated with a simulation bandwidth of 1280GHz for single channel. For the simulation of a WDM system, we have launched five channels with a channel spacing of 200GHz and the wavelength of the central channel is 1.55μm. The rest of the parameters are the same as that used in the single channel simulation. Figs. 4.3 and 4.4 show the comparison of Q-factor for single channel and WDM transmission systems, respectively. As can be seen, there is a significant improvement in system performance using OPC followed by $\hat{\mathbf{K}}$ (System IV). An interesting fact is that Q-factor increases with launch power for System IV unlike other systems. If the nonlinear impairments are much smaller than that due to amplifier noise, Q-factor scales roughly with square root of the launch power, in qualitative agreement with the result for System IV, implying that nonlinear impairments are absent for System IV.

4.4 Conclusion

We proposed a new way to design the inverse of fiber systems based on the theory of pth-order inverse of Volterra expansion. For a fully dispersion compensated fiber system $\mathbf{H}$ with a second-order dispersion profile $\beta_2(z)$ and a total length L, the inverse is constructed using an OPC followed by a system $\hat{\mathbf{K}}$ with an inverted seconder-order dispersion profile

$-\beta_2(z-L)$, while keeping all the other parameters the same. The simulation results show that for both single channel and WDM systems, there is a significant improvement in Q factor with our design, especially when fiber nonlinearities are the main source of system noise.

Chapter 5

Adaptive Cancelation of Nonlinear Intersymbol Interference for Optical Fiber Systems

5.1 Introduction

The impairments of the optical fiber channel can be treated as intersymbol interferences (ISI). The source of intersymbol interference include nonlinearity in the laser transmitter, chromatic dispersion in systems operating at wavelengths other than the zero dispersion of the fiber, polarization mode dispersion, bandwidth limitation in the receiver and mode partition fluctuations. Some of these impairments, such as chromatic dispersion, can be compensated optically. Dispersion compensating fiber (DC) and optical polarization-mode dispersion (PMD) compensators are examples of such optical components. Optical compensation techniques have the advantage of not requiring high-speed IC technology. However, due to a lack of flexibility and the hight cost of these solutions, electronic compensation may be a better choice. Compared with optical compensation, electronic compensation methods have much less dynamic range but offer low first installed cost and adaptive dispersion compensation. In this Chapter, we examine a nonlinear ISI canceler based on Volterra theory, which was proposed first for voiceband data transmission [17], and apply it to optical fiber systems. The canceler mitigates nonlinearities by processing the output of a linear equalizer (LE). The nonlinear ISI caused by both the postcursor and precursor is compensated by making tentative decision. The simulation results show that it improves the system performance by 1dB.

5.2 The Nonlinear Cancelation of ISI

5.2.1 The Nonlinear Channel Model

The input signal $x(t)$ is transmitted over the nonlinear fiber channel.

$$x(t) = \sum_{n=-\infty}^{n=\infty} a_n A_0 e^{-\frac{(t-nT)^2}{2\sigma^2}}, \tag{5.1}$$

where $a_n \in \{0, 1\}$ is the bit pattern at time nT, the input signal is a series of Gaussian pulses with amplitude A_0. Due to fiber nonlinearities, nonlinear ISI is introduced at the

channel output. The output signal field $y(t)$ is given by

$$y(t) = \int h_1(\tau)x(t-\tau)d\tau + \iiint h_3(\tau_1,\tau_2,\tau_3)x(t-\tau_1)x^*(t-\tau_2)x(t-\tau_3)d\tau_1 d\tau_2 d\tau_3, \quad (5.2)$$

where $h_1(t)$ and $h_3(t_1,t_2,t_3)$ are the first- and third-order Volterra kernels in time domain. At sampling time NT

$$y(NT) = \sum_{n=-\infty}^{\infty} a_n B_n + \sum_{n_1=-\infty}^{n_1=\infty}\sum_{n_2=-\infty}^{n_2=\infty}\sum_{n_3=-\infty}^{n_3=\infty} a_{n_1}a_{n_2}a_{n_3}C_{n_1,n_2,n_3}, \quad (5.3)$$

where

$$B_n = \int A_0 h_1(\tau) e^{-\frac{(NT-\tau-nT)^2}{2\sigma^2}} d\tau \quad (5.4)$$

$$C_{n_1,n_2,n_3} = \iiint h_3(\tau_1,\tau_2,\tau_3)A_0|A_0|^2 e^{-\frac{(NT-\tau_1-nT)^2+(NT-\tau_2-nT)^2+(NT-\tau_3-nT)^2}{2\sigma^2}} d\tau_1 d\tau_2 d\tau_3 \quad (5.5)$$

B_n and C_{n_1,n_2,n_3} can be seen as constants for a given system, and can be decided adaptively.

After the photo-detector, the electrical current(assuming unit responsitivity for the photodiode) is

$$\begin{aligned} |y(NT)|^2 = {} & a_0|B_0|^2 + \sum_{n=-\infty, n\neq 0}^{\infty} a_n|B_n|^2 \\ & + \sum_{n_1=-\infty}^{\infty}\sum_{n_2=-\infty, n_2\neq n_1}^{\infty} a_{n_1}a_{n_2}B_{n_1}B_{n_2}^* \\ & + \sum_{n=-\infty}^{n=\infty}\sum_{n_1=-\infty}^{n_1=\infty}\sum_{n_2=-\infty}^{n_2=\infty}\sum_{n_3=-\infty}^{n_3=\infty} a_n a_{n_1}a_{n_2}a_{n_3}\cdot 2\mathrm{Re}\left[B_n C_{n_1,n_2,n_3}^*\right] \\ & + \mathcal{O}(\gamma^2). \end{aligned} \quad (5.6)$$

The first term is the desired signal, the second term is the linear distortion which can be compensated by linear equalizer, the third and fourth term are nonlinear distortion, and $\mathcal{O}(\gamma^2)$ can be ignored. The cancelation of nonlinear ISI can be achieved by subtracting the nonlinear term from $y(NT)$

$$Y_{NL} = \sum_{n_1=-\infty}^{\infty}\sum_{n_2=-\infty, n_2\neq n_1}^{\infty} a_{n_1}a_{n_2}D_{n_1,n_2} + \sum_{n=-\infty}^{n=\infty}\sum_{n_1=-\infty}^{n_1=\infty}\sum_{n_2=-\infty}^{n_2=\infty}\sum_{n_3=-\infty}^{n_3=\infty} a_n a_{n_1}a_{n_2}a_{n_3}E_{n,n_1,n_2,n_3} \quad (5.7)$$

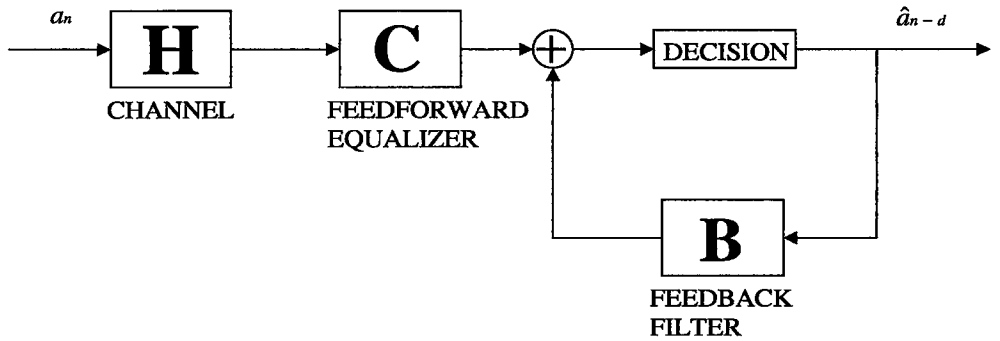

Figure 5.1: Decision-feedback structure

where

$$D_{n_1,n_2} = B_{n_1} B^*_{n_2}. \tag{5.8}$$

$$E_{n,n_1,n_2,n_3} = 2\mathrm{Re}\left[B_n C^*_{n_1,n_2,n_3}\right], \tag{5.9}$$

which is a sum of cross-product terms of the decisions $\{a_n\}$ both before and after the current bit.

5.2.2 The Nonlinear Cancelation Scheme

The decision-feedback structure, proposed by Falconer [18], is shown in Fig. 5.1, which is a combination of a feedforward equalizer **C** and a feedback filter **B**. The forward equalizer **C** reshapes the input pulse to suppress the sidelobes preceding the main lobe, and the decision feedback filter **B** cancels the ISI caused by postcursors. The model is based on the assumption that the input to the decision-feed back filter **B** consists of correct data symbols. With this assumption, the model can be reformulated as shown in Fig. 5.2, and this makes no change in the conceptual view. In this way, the system now is able to deal with the entire ISI from precursors, postcursors, and their cross products. Biglieri [17] extend this scheme to a practical nonlinear cancelation scheme shown in Fig. 5.3. In Fig. 5.3, **LE** is a linear equalizer that is used to eliminate linear distortion, and at the same

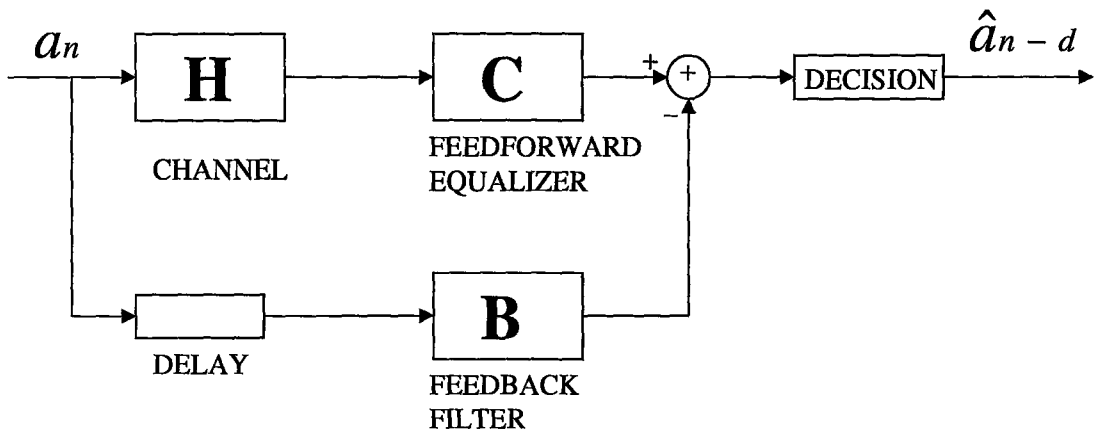

Figure 5.2: Reformulated decision-feedback structure

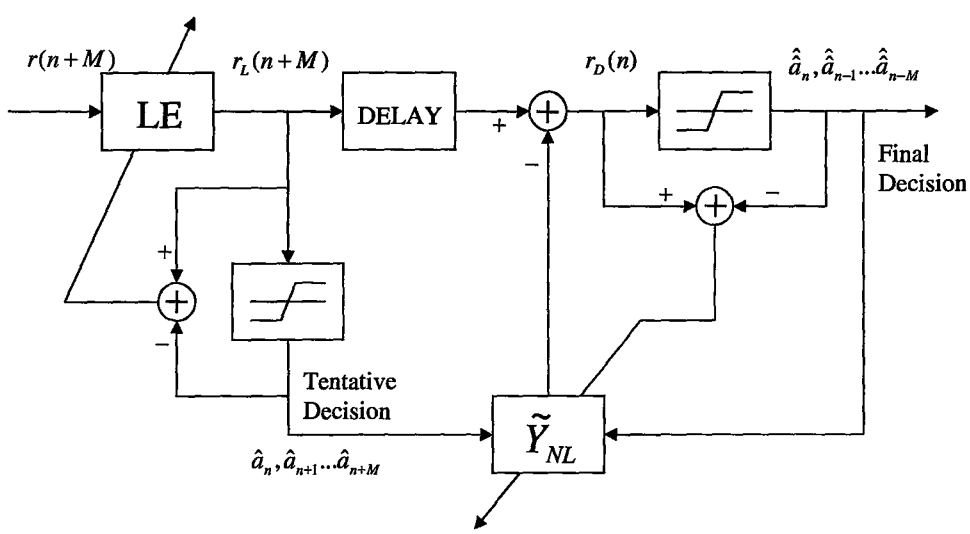

Figure 5.3: Practical nonlinear cancelation scheme

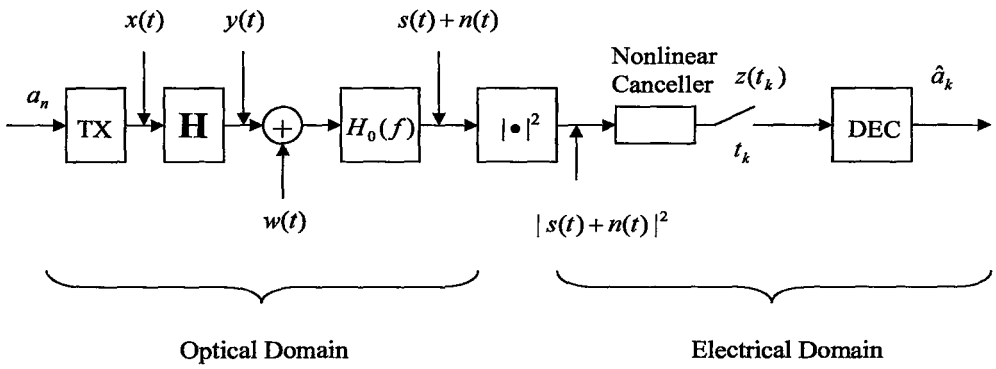

Figure 5.4: Block diagram of the detection scheme

time, improve the accuracy of tentative decision. We delay output of **LE**, $x_L(n+M)$, by M, and then subtract the nonlinear part of ISI, $\tilde{Y}_{NL}$, which is the cross product of both precursors and postcursors, and in the form of eq. (5.7). The resulted signal $x_D(n)$ is used to make the final decision. The coefficients for the linear equalizer LE and the nonlinear canceler $\tilde{Y}_{NL}$ are chose adaptively.

The canceler shown in Fig. 5.3 is supposed to cancel the entire nonlinear ISI created by the combined effect of the channel and an LE. It can be viewed as a modified decision-feedback technique where the limitation of causality is solved by using tentative decisions rather than final decisions to synthesize the estimated nonlinear ISI.

5.3 Evaluation of the Error Probability

Forestieri [57] proposed a novel approach to analytically evaluate the bit error probability in preamplified direct detection systems, which takes into account arbitrary signal pulse shape, chirping, filtering at the transmitter and the receiver, both pre- and postdetection, and channel impairments, and is well suited for the performance analysis of the nonlinear canceler in the previous section.

The system is shown in Fig. 5.4. Given a N-bit sequence $\{a_n\}$ to be transmitted, and

$p(t)$ is the elementary pulse, the transmitted signal is expressed as

$$d(t) = \sum_{i=0}^{N-1} a_i p(t - iT) \tag{5.10}$$

we expand it to be periodic repetition with period NT

$$x(t) = \sum_{n=-\infty}^{\infty} d(t - nNT). \tag{5.11}$$

When N is sufficiently large, $x(t)$ in eq. (5.11) is a pseudorandom signal which is tractable mathematically while retaining physical properties close to reality. Due to its periodicity, $x(t)$ can be expand in Fourier series

$$x(t) = \sum_{\ell=-\infty}^{\infty} x_\ell e^{j2\pi\ell t/NT} \tag{5.12}$$

The overall impulse response of the pre- and postdetection filters at the receiver has a finite time duration T_0, so the sample $y(t_k)$ is solely determined by the values that the input waveform in the time interval $(t_k - T_0, t_k)$. An exact description of the input noise waveform in $(t_k - T_0, t_k)$ is a sufficient statistics. So we can write a Karhunen-Loève expansion for the noise $w(t)$ in the interval $t_k - T_0 < t < t_k$ only, and as $w(t)$ is additive white gaussian noise (AWGN), we can choose any orthogonal base,

$$\{\varphi_m(t) = (1/\sqrt{T_0})e^{j2\pi m(t-t_k+T_0)/T_0}\}_{m=-\infty}^{\infty}. \tag{5.13}$$

So the relevant noise process becomes

$$w(t) = \sum_{m=-\infty}^{\infty} w_m \varphi_m(t), t_k - T_0 < t < t_k, \tag{5.14}$$

where w_m are complex independent and identically distributed (i.i.d.) Gaussian random variable (r.v.) with zero mean and variance of $N_0/2$ for in-phase and quadrature components. For convenience, $w(t)$ is written as

$$w(t) = \sum_{m=-\infty}^{\infty} w_m e^{j2\pi m(t-t_k+T_0)/T_0}, t_k - T_0 < t < t_k \tag{5.15}$$

where w_m are complex i.i.d. Gaussian r.v. with zero mean and in-phase and quadrature components of variance

$$\sigma^2 = \frac{N_0}{2T_0}. \tag{5.16}$$

The value of T_0 depends upon the optical and postdetection filters.

We now derive an expression for the sample $z(t_k)$ at the input of the decision device. By retaining only the significant harmonics, the quadratic detector input signal component in Fig. 5.4 is

$$s(t) = \sum_{\ell=-L}^{L} s_\ell e^{j2\pi\ell t/NT} \tag{5.17}$$

where

$$L = \eta N B_{oN} T \tag{5.18}$$

B_{oN} is the noise equivalent bandwidth of $H_o(f)$, the value of η to be used in eq. (5.17) depends on the optical filter shape and may be chosen such that $\sum_{|\ell|>L} |s_\ell|^2 < \varepsilon E_b$, with ε small enough, or may be found be successive trials. The quadratic detector input noise can be written as

$$n(t) = \sum_{m=-M}^{M} n_m e^{j2\pi m(t-t_k+T_0)T_0}, \text{for} t_k - T_0 \leq t \leq t_k, \tag{5.19}$$

where

$$M = \eta B_{oN} T_0 \tag{5.20}$$

$$n_m = w_m H_o\left(\frac{m}{T_0}\right) \tag{5.21}$$

and w_m are as in 5.15. Then the quadratic detector output signal in Fig. 5.4, in the time interval $t_k - T_0 \leq t \leq t_k$, may be written as

$$\begin{aligned}|s(t)+n(t)|^2 = &\sum_{\ell=-2L}^{2L} c_\ell e^{j2\pi\ell t/NT} \\ &+ \sum_{\ell=-L}^{L}\sum_{m=-M}^{M} s_\ell n_m^* \exp\left\{j2\pi\left[\frac{\ell t}{NT} - \frac{m(t-t_k+T_0)}{T_0}\right]\right\} \\ &+ \sum_{\ell=-L}^{L}\sum_{m=-M}^{M} s_\ell^* n_m \exp\left\{-j2\pi\left[\frac{\ell t}{NT} - \frac{m(t-t_k+T_0)}{T_0}\right]\right\} \\ &+ \sum_{\ell=-M}^{M}\sum_{m=-M}^{M} n_\ell n_m^* \exp\left\{j2\pi(\ell-m)\frac{t-t_k+T_0}{T_0}\right\},\end{aligned} \tag{5.22}$$

where c_ℓ is the autocorrelation of the coefficients of the Fourier series expansion of the signal $s(t)$ in eq. (5.17)

$$c_\ell = \sum_{k=\max(-L,\ell-L)}^{\min(L,\ell+L)} s_k s_{k-\ell}^* \tag{5.23}$$

The nonlinear canceler is composed of a LE with transfer function $H_R(f)$, and then subtract a constant $\tilde{Y}_{NL}(t_k)$ which is determined by input bit pattern. The sample $z(t_k)$ in Fig. 5.4 may be written as

$$\begin{aligned}z(t_k) = &\sum_{\ell=-2L}^{2L} c_\ell H_R\left(\frac{\ell}{NT}\right) e^{j2\pi\ell t_k/NT} \\ &+ \sum_{\ell=-L}^{L}\sum_{m=-M}^{M} s_\ell n_m^* H_R\left(\frac{\ell}{NT} - \frac{m}{T_0}\right) e^{j2\pi\ell t_k/NT} \\ &+ \sum_{\ell=-L}^{L}\sum_{m=-M}^{M} s_\ell^* n_m H_R^*\left(\frac{\ell}{NT} - \frac{m}{T_0}\right) e^{-j2\pi\ell t_k/NT} \\ &+ \sum_{\ell=-M}^{M}\sum_{m=-M}^{M} n_\ell n_m^* H_R\left(\frac{\ell-m}{T_0}\right) - \tilde{Y}_{NL}(t_k).\end{aligned} \tag{5.24}$$

where $\tilde{Y}_{NL}(t_k)$ has the structure shown in eq. 5.7. However, it is calculated adaptively. Reformulate eq. 5.24 in compact matrix notation, as

$$z(t_k) = \mathbf{n}^{T*} Q \mathbf{n} + \mathbf{n}^{T*}\mathbf{v} + \mathbf{v}^{T*}\mathbf{n} + c - \tilde{Y}_{NL}(t_k). \tag{5.25}$$

where $\mathbf{n}$ is a column vector whose $2M+1$ components are

$$n_i = w_{i-M-1} H_o\left(\frac{i-M-1}{T_0}\right), \qquad i = 1, 2, \cdots, 2M+1 \tag{5.26}$$

w_i being as in eq. (5.15), Q is a $(2M+1) \times (2M+1)$ matrix whose elements are

$$q_{ij} = H_R\left(\frac{i-j}{T_0}\right), \qquad i, j = 1, 2, \cdots, 2M+1 \tag{5.27}$$

and, for the Hermitian symmetry of $H_R(f)$, they are such that $q_{ij} = q_{ji}^*$ (i.e. Q is Hermitian), $\mathbf{v}$ is a column vector whose $2M+1$ components are

$$v_i = \sum_{\ell=-L}^{L} s_\ell H_R\left(\frac{\ell}{NT} - \frac{i-M-1}{T_0}\right) e^{j2\pi\ell t_k/NT}, \qquad i = 1, 2, \cdots, 2M+1 \tag{5.28}$$

and finally c is the constant

$$c = \sum_{\ell=-2L}^{2L} c_\ell H_R\left(\frac{\ell}{NT}\right) e^{j2\pi\ell t_k/NT}. \tag{5.29}$$

$\mathbf{n}$ is a complex Gaussian random vector with zero mean and diagonal covariance matrix

$$E\{\mathbf{n}^*\mathbf{n}^T\} = 2\sigma^2 \mathrm{diag}\{|h_i|^2\}, \tag{5.30}$$

where σ^2 is as in eq. (5.16), $\mathrm{diag}\{c_i\}$ is by definition a diagonal matrix whose diagonal elements c_{ii} are $c_{ii} = c_i, i = 1, 2, \cdots$, and

$$h_i \triangleq H_o\left(\frac{i-M-1}{T_0}\right). \tag{5.31}$$

As the statistics of the filtered noise do not depend on the optical filter phase response but only on its amplitude response, by convenience we can define the matrix H as follows

$$H \triangleq \mathrm{diag}\{|h_i|\}, \tag{5.32}$$

and by using the transformation

$$\mathbf{n} = H\mathbf{w}, \tag{5.33}$$

where the equal sign is to be interpreted in the sense that both sides are statistically equivalent. We can write

$$\mathbf{n}^{T*}Q\mathbf{n} = \mathbf{w}^{T*}H^{T*}QH\mathbf{w} = \mathbf{w}^{T*}A\mathbf{w}, \tag{5.34}$$

with

$$A = H^{T*}QH. \tag{5.35}$$

still Hermitian. Following the discussion of A in [57], A can be diagonalized by the unitary matrix U formed by its normalized eigenvectors arranged in the same order of their corresponding eigenvalues λ_i

$$A = U\Lambda U^{T*}, \tag{5.36}$$

where

$$\Lambda = \text{diag}\{\lambda_i\}. \tag{5.37}$$

Then we can write

$$\mathbf{n}^{T*}Q\mathbf{n} = \mathbf{w}^{T*}U\Lambda U^{T*}\mathbf{w} = \mathbf{z}^{T*}\Lambda\mathbf{z}, \tag{5.38}$$

with

$$\mathbf{z} = U^{T*}\mathbf{w} = U^{T*}H^{-1}\mathbf{n}, \tag{5.39}$$

and

$$E\{\mathbf{z}^*\mathbf{z}^T\} = 2\sigma^2 I, \tag{5.40}$$

which means that the $\mathbf{z}$ components are independent complex Gaussian r.v. with zero mean and same variance. By defining the vector

$$\mathbf{b} \triangleq= U^{T*}H^T\mathbf{v}, \tag{5.41}$$

and summing and subtracting to eq. (5.25) the term $\mathbf{b}^{T*}\Lambda^{-1}\mathbf{b}$, the sample $z(t_k)$ may be written as

$$\begin{aligned} z(t_k) &= \mathbf{z}^{T*}\Lambda\mathbf{z} + \mathbf{z}^{T*}\mathbf{b} + \mathbf{b}^{T*}\mathbf{z} + c + \mathbf{b}^{T*}\Lambda^{-1}\mathbf{b} - \mathbf{b}^{T*}\Lambda^{-1}\mathbf{b} - \tilde{Y}_{NL}(t_k) \\ &= (\mathbf{z} + \Lambda^{-1}\mathbf{b})^{T*}\Lambda(\mathbf{z} + \Lambda^{-1}\mathbf{b}) + c - \mathbf{b}^{T*}\Lambda^{-1}\mathbf{b} - \tilde{Y}_{NL}(t_k) \\ &= \sum_{i=1}^{2M+1} \lambda_i \left| z_i + \frac{b_i}{\lambda_i} \right|^2 + \sum_{\ell=-2L}^{2L} c_\ell H_R\left(\frac{\ell}{NT}\right) e^{j2\pi\ell t_k/NT} - \sum_{i=1}^{2M+1} \frac{|b_i|^2}{\lambda_i} - \tilde{Y}_{NL}(t_k) \end{aligned} \quad (5.42)$$

The sample $z(t_k)$ at the input of the decision device may be written as

$$z(t_k) = d_k + r_k - \tilde{Y}_{NL}(t_k), \quad (5.43)$$

where

$$d_k \triangleq \sum_{\ell=-2L}^{2L} c_\ell H_R\left(\frac{\ell}{NT}\right) e^{j2\pi\ell t_k/NT}, \quad (5.44)$$

is the signal term, while r_k is the noise term which may be written as

$$r_k = n_k - \nu_k, \quad (5.45)$$

where

$$n_k \triangleq \sum_{i=1}^{2M+1} \lambda_i \left| z_i + \frac{b_i}{\lambda_i} \right|^2, \quad (5.46)$$

$$\nu_k \triangleq \sum_{i=1}^{2M+1} \frac{|b_i|^2}{\lambda_i}. \quad (5.47)$$

The complex random variables $z_i = z_{Pi} + jz_{Qi}$ are zero mean Gaussian with independent in-phase and quadrature components of variance σ^2 as in eq. (5.15), b_i are the components of the complex vector $\mathbf{b}$ given in eq. (5.41). The noise sample n_k is a noncentral quadratic form of Gaussian random variables, for which it can be easily shown that its moment generating function (MGF) is

$$\Psi_{n_k}(s) = \prod_{i=1}^{2M+1} \frac{\exp\left(\frac{\alpha_i s}{1-\beta_i s}\right)}{1-\beta_i s}, \quad (5.48)$$

where

$$\alpha_i \triangleq \frac{|b_i|^2}{\lambda_i}, \tag{5.49}$$

$$\beta_i \triangleq 2\lambda_i\sigma^2, \tag{5.50}$$

$$\eta_{n_k} = \sum_{i=1}^{2M+1}(\alpha_i + \beta_i) = \sum_{i=1}^{2M+1}\left(2\lambda_i\sigma^2 + \frac{|b_i|^2}{\lambda_i}\right), \tag{5.51}$$

$$\sigma_{n_k}^2 = \sum_{i=1}^{2M+1}\beta_i(2\alpha_i + \beta_i) = \sum_{i=1}^{2M+1}4\sigma^2(\lambda_i^2\sigma^2 + |b_i|^2). \tag{5.52}$$

Setting the decision threshold to γ_{th}, the probability of error at the sampling time t_k, conditional upon the information sequence $\{a_n\}$ is

$$P(e_k|\{a_n\}) = \begin{cases} P\{y(t_k) < \gamma_{th} + \tilde{Y}_{NL}(t_k)\} = P\{n_k < \xi_k\}, & a_k = 1 \\ P\{y(t_k) > \gamma_{th} + \tilde{Y}_{NL}(t_k\} = P\{n_k > \xi_k\}, & a_k = 0, \end{cases} \tag{5.53}$$

where

$$\xi_k = \gamma_{th} + \tilde{Y}_{NL}(t_k) - d_k + \nu_k, \tag{5.54}$$

and the average probability of error P_e can be expressed as

$$P_e = \frac{1}{N}\sum_{k=0}^{N-1}P(e_k|\{a_n\}). \tag{5.55}$$

The probabilities that appear in eq. (5.51) may be evaluated as

$$P\{n_k > \xi_k\} = \frac{1}{2\pi j}\int_{u_0-j\infty}^{u_0+j\infty}\frac{\Psi(s)}{s}e^{-s\xi_k}ds, 0 < u_0 < \frac{1}{\max\beta_i^+} \tag{5.56}$$

$$P\{n_k < \xi_k\} = -\frac{1}{2\pi j}\int_{u_0-j\infty}^{u_0+j\infty}\frac{\Psi(s)}{s}e^{-s\xi_k}ds, -\frac{1}{\max|\beta_i^-|} < u_0 < 0 \tag{5.57}$$

where β_i^+ and β_i^- stands for the positive and negative β_is in eq. (5.50), respectively. If all β_is are positive then the range in eq. (5.57) is to be interpreted as $-\infty < u_0 < 0$. It can be shown that the integrand in eq. (5.56) and eq. (5.57) has two saddle points $u_0^- < 0$ and $u_0^+ > 0$ on the real s-axis which, once determined, can be used to obtain the closed

form saddlepoint approximation for the bit error probability. By writing eq. (5.48) as $\Psi_{n_k}(s) = \exp[\Phi_{n_k}(s)]$ and expanding $\Phi_{n_k}(s)$ in power series about $u_0\pm$ retaining terms up to s^2, eq. (5.56) and eq. (5.57) can be reduced to Gaussian integrals, which are evaluated to give the saddlepoint approximation

$$P\{n_k \gtrless\} \simeq \pm\frac{\exp[\Phi_{n_k}(u_0^{\pm})]}{\sqrt{2\pi\Phi''_{n_k}(u_0^{\pm})}} = \frac{[\Psi_{n_k}(u_0^{\pm})]^{3/2}e^{-u_0^{\pm}\xi_k}}{\sqrt{2\pi[(u_0^{\pm})^2\Phi''_{n_k}(u_0^{\pm}) + \Phi_{n_k}(u_0^{\pm})]}}, \tag{5.58}$$

where Φ''_{n_k} stands for the seconde derivative of Φ_{n_k} and u_0^+ or u_0^- must be used for the $>$ or $<$ sign, respectively.

5.4 Simulation Result

Fig. 5.5 shows the comparison of bit-error rate (BER) for uncompensated, linearly compensated, and nonlinearly compensated schemes. Numerical simulations are carried out with the following parameters: bit rate $B = 40$Gb/s, and $\lambda = 1.55\mu$m. The Gaussian pulses with FWHM=12.5ps are launched to a dispersion managed fiber with nonlinear coefficient= $0.01\text{W}^{-1}\text{km}^{-1}$ and loss $\alpha = 0.2$dB/km, amplifier spacing = 80km. Dispersion management is done by using a 40-km-long single mode fiber with $D = 17\text{ps}/(\text{nm}\cdot\text{km})$, followed by reverse dispersion fiber with $D = 14.5\text{ps}/(\text{nm}\cdot\text{km})$, which is precompensated by a 7.5-km-long single mode fiber with $D = -100\text{ps}/(\text{nm}\cdot\text{km})$, and postcompensated by a 2.5-km-long single mode fiber with $D = -100\text{ps}/(\text{nm}\cdot\text{km})$. 16384 bits are simulated, and the optical filter is assumed to be ideal bandpass filter with bandwidth of 80GHz. The nonlinear canceler in Fig. 5.4 is constructed as in Fig. 5.3. We choose 8 taps for the linear equalizer and the delay M of the canceler shown in Fig. 5.3 is chosen as 2. The coefficients for the linear equalizer and nonlinear canceler are chosen adaptively using recursive least squares (RLS) adaptive algorithm. From Fig. 5.5, we can see that BER can be reduced a little using linear compensation. However, using the nonlinear cancelation scheme, substantial reduction in BER is possible.

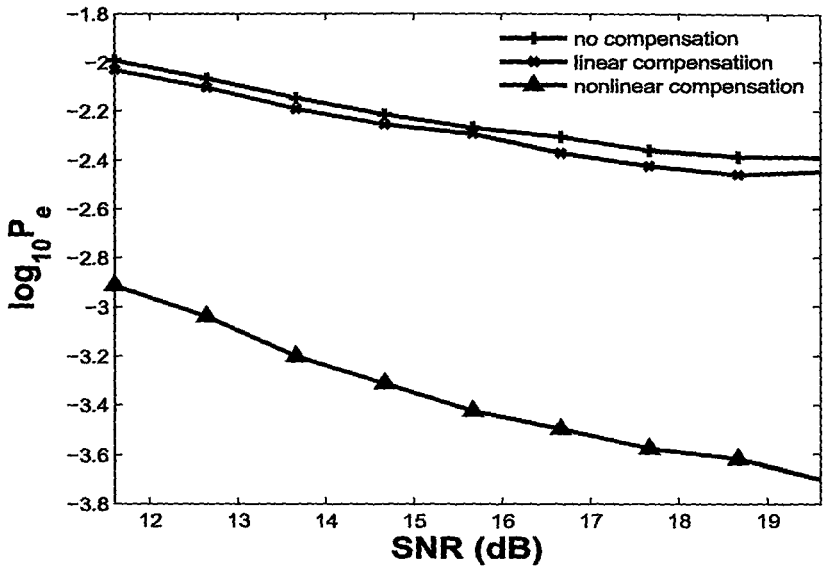

Figure 5.5: Comparison of BER for uncompensated, linearly compensated, and nonlinearly compensated schemes

5.5 Conclusion

A nonlinear ISI canceler based on Volterra theory is examined in this chapter. The scheme adaptively synthesizes a Volterra series model of the nonlinear interference impulse response with the use of tentative symbol decision. The simulation result shows that BER is reduced by approximately 1dB by using nonlinear compensation schemes.

Chapter 6

Conclusion

We have proposed an easy way to design the inverse of fiber systems based on the theory of pth-order inverse of Volterra expansion. For a fully dispersion compensated fiber system $\mathbf{H}$ with a second-order dispersion profile $\beta_2(z)$ and a total length of L, the inverse is approximated by a system $\hat{\mathbf{K}}$ with an inverted seconder-order dispersion profile $-\beta_2(z-L)$, while keeping all the other parameters the same. Our simulation shows that the Q factor is improved with our design, especially when fiber nonlinearities are the main source of system noise.

We then further developed the above model by adding an OPC in the middle of the span. For a fully dispersion compensated fiber system $\mathbf{H}$ with a second-order dispersion profile $\beta_2(z)$ and a total length L, the inverse is constructed using an OPC followed by a system $\hat{\mathbf{K}}$ with an inverted seconder-order dispersion profile $-\beta_2(z-L)$, while keeping all the other parameters the same. The simulation results show that for both single channel and WDM systems, there is a significant improvement in Q factor with our design, especially when fiber nonlinearities are the main source of system noise.

We also examined an electronic compensation scheme based on Volterra theory. The scheme adaptively synthesizes a Volterra series model of the nonlinear interference impulse response with the use of tentative symbol decision. The simulation result shows that BER is reduced by approximately 2dB by using the nonlinear compensation scheme.

Bibliography

[1] G. P. Agrawal, Nonlinear Fiber Optics, New York: Academic, 2001.

[2] G. P. Agrawal, Fiber-Optic Communication Systems, New York: Wiley, 2002.

[3] J. L. Rebola, and A. V. T. Cartaxo, Power Penalty Assessment in Optically Preamplified Recievers with Arbitrary Optical Filtering and Signal-Dependent Noise Dominance, J. Lightwave Technol., vol. 20, pp. 401-408, Mar. 2002.

[4] R. Giles, and T. Li, Optical Amplifiers Transform Long-distance Lightwave Telecommunications, Proceedings of the IEEE, vol. 84, pp. 870-883, June 1996.

[5] M. J. Yadlowsky, E. M. Deliso, and V. L. Da SiLva, Optical Fibers and Amplifers for WDM Systems, Proceedings of the IEEE, vol. 85, pp. 1765-1779, Nov. 1997.

[6] L. Grüner-Nielsen, M. Wandel, P. Kristensen, C. JØrgensen, L. V. JØrgensen, B. Edvold, B. Pálsdóttir, and D. Jakobsen, Dispersion-Compensating Fibers, J. Lightwave Technol., vol. 23, pp. 3566-3579, 2005.

[7] B. Jopson and A. Gnauck, Dispersion Compensation for Optical Fiber Systems, IEEE Communications Magazine, vol.33, pp. 96-102 June 1995.

[8] J. Toulouse, Optical Nonlinearities in Fibers: Review, Recent Examples, and Systems Applications, J. Lightwave Technol., vol. 23, pp. 3625-3641, Nov. 2005.

[9] P. V. Mamyshev and N. A. Mamysheva, Pulse-overlapped Dispersion-managed Data Transmission and Intrachannel Four-wave mixing, Optics Letters, vol. 24, pp. 1454-1456, Nov, 1999.

[10] R. H. Stolen, Nonlinearity in Fiber Transmission, Proc. Proc.IEEE, vol. 68, pp. 1232-1236, Oct. 1986.

[11] D. Marcuse, RMS Width of Pulse in Nonlinear Dispersive Fibers, J. Lightwave Technol., vol. 10, pp. 17-21, Jan. 1992.

[12] A. R. Chraplyvy, Limitations on Lightwave Communications Imposed by Optical Fiber Nonlinearities, J. Lightwave Technol., vol. 8, pp. 1548-1557, Oct. 1990.

[13] A. Mecozzi, C. B. Clausen, and M. Shtaif, System Impact of Intrachannel Nonlinear Effects in Highly Dispersed Optical Pulse Transmission, IEEE Photonics Technol. Lett., vol.12, pp. 1633-1635, Dec. 2000.

[14] H. A. Haus, Group Velocity, Energy, and Polarization Mode Dispersion, J. Opt. Soc. Amer. B, vol. 16, pp. 1863-1867, Nov. 1999.

[15] M. Karlsson, Polarization Mode Dispersion-induced Pulse Broadening in Optical Fibers, Opt. Lett., vol. 23, pp. 688-690, May 1998.

[16] G. J. Foschini, and C. D. Poole, Statistical Theory of Polarization Dispersion in Single-Mode Fibers, J. Lightwave Technol., vol. 9, pp. 1439-1456, Nov. 1991.

[17] E. Biglieri, and A. Gersho, R. D. Gitlin, Adaptive Cancellation of Nonlinear Intersymbol Interference for Voiceband Data Transmission, IEEE Journal on Selected Areas in Communications, vol. SAC-2, Sept. 1984.

[18] D. D. Falconer, Adaptive Equalization of Channel Nonlinearities in QAM Data Transmission Systems, Bell Syst. Tech. J., vol. 57, no. 7, pp. 2589-2611, Sept. 1978.

[19] S. Kasturia, and J. H. Winters, Techniques for High-Speed Implementation of Nonlinear Cancellation, IEEE Selected Areas in Communications, vol. 9, pp. 711-717, June 1991.

[20] J. H. Winters, and S. Kasturia, Adaptive Nonlinear Cancellation for High-speed Fiber-optic Systems, J. Lightwave Technol., vol. 10, pp. 971-977, July 1992.

[21] K. Roberts, P. M. Watts, V. Mikhailov, M. Glick, and P. Bayvel, Electronic Dispersion Compensation by Signal predistortion Using Digital Processing and a Dual-Drive Mach-Zehnder Modulator, IEEE Photonics Technol., vol. 17, pp. 714-716, March. 2005

[22] K. Roberts, C. Li, L. Strawczynski, M. O'Sullivan, and I. Hardcastle, Electronic Precompensation of Optical Nonlinearity, IEEE Photonics Technol., vol. 18, pp. 403-405, Jan. 2006

[23] K. Kikuchi, and C. Lorattanasane, Compensation for Pulse Waveform Distortion in Ultra-Long Distance Optical Communication Systems by Using Midway Opitcal Phase Conjugator, IEEE Photonics Technol. Lett., vol.6, pp. 104-105, Jan. 1994.

[24] A. Mecozzi, C. B. Clausen, M. Shtaif, Sang-Gyu Park and A. H. Gnauck, Cancellation of Timing and Amplitude Jitter in Symmetric Links Using Highly Dispersed Pulses, IEEE Photonics Technol. Lett., vol.13, pp. 445-447, Oct. 2001.

[25] A. G. Striegler and B. Schmauss, Compensation of Intrachannel Effects in Symmetric Dispersion-managed Transmission Systems, J. Lightwave Technol., vol. 22, pp. 1877-1882, Aug. 2004.

[26] S. Kumar and D. Yang, Second Order Theory for Self-phase Modulation and Cross-phase Modulation in Optical Fibers, J. Lightwave Technol., vol.23, pp. 2073-2080, June. 2005.

[27] A. Yariv, D. Fekete and D. M. Pepper, Compensation for Channel Dispersion by Nonlinear Optical Phase Conjugation, Opt. Lett., vol.4, pp. 52-54, Feb. 1979.

[28] S. Watanabe, Compensation of Phase Fluctuation in A Transmission Line by Optical Phase Conjugation, Opt. Lett., vol.17, pp. 1355-1357, 1993.

[29] D. M. Pepper and A. Yariv, Compensation for Phase Distortions in Nonlinear Media by Phase Conjuation, Opt. Lett., vol.5, pp. 59-60, Feb. 1980.

[30] S. Watanabe, T. Chikama, G. Ishikawa, T. Terahara, and H. Kuwahara, Compensation of Pulse Shape Distortion Due to Chromatic Dispersion and Kerr Effect by Optical phase conjuation, IEEE Photonics Technol. Lett., vol.5, pp. 1241-1243, 1993.

[31] A. Yariv, Phase Conjugate Optics and Real-time Holography, IEEE J. Quantum Electron., vol.QE-14, pp. 650-660, 1978.

[32] R. A. Fisher, B. R. Suydam and D. Yevick, Optical Phase Conjugation for Time-domain Undoing of Dispersive Self-phase-modulation Effects, Opt. Lett., vol.8, pp. 611-613, 1983.

[33] W. Pieper and C. Kurtzke, R. Schnabel, D. Breuer, R. Ludwig, K. Petermann, and H. G. Weber, Nonlinearity-insensitive Standard-fiber Transmission Based on Optical-phase Conjuation in A Semiconductor-laser Amplifer, Electron. Lett., vol.30, pp. 724-726, 1994.

[34] K. Kikuchi and C. Lorattanasane, Compensation for Phase Waveform Distortion in Ultra-long Distance Optical Communication Systems by Using Nonlinear Optical Phase Conjugator, in OAA'93, Yokohama, Japan, 1993, Paper SuC1, pp. 22-25.

[35] C. Kurtzke and A. Gnauck, How to Increse Capacity Beyond 200 Tbit/skm Without Solitons, in ECOC'93, 1993, Paper ThC 12.12, pp. 45-48.

[36] S. Watanabe, G. Ishikawa, T. Naito, and T. Chikama, Generation of Optical Phase-conjugate Waves and Compensation for Pusle Shape Distortion in A Single-mode Fiber, J. Lightwave Technol. vol. 12, pp. 2139-2146, 1994.

[37] S. Watanabe and M. Shirasaki, Exact Compensation for Both Chromatic Dispersion and Kerr Effect in A Transmission Fiber Using Optical Phase Conjugation, J. Lighwave Technol., vol. 14, pp. 243-248, March 1996.

[38] P. Kaewplung, T. Angkaew, and K. Kikuchi, Simultaneous Suppression of Third-Order Dispersion and Sideband Instablity in Single-Channel Optical Fiber Transmission by Midway Optical Phase Conjugation Employing Higher Order Dispersion Management, J. Lighwave Technol., vol. 21, pp. 1465-1473, June 2003.

[39] I. Brener, B. Mikkelsen, K. Rottwitt, W. Burkett, G. Raybon, J. B. Stark, K. Parameswaran, M. H. Chou, M. M. Fejer, E. E. Chaban, R. Harel, D. L. Philen, and S. Kosinski, Cancellation of All Kerr Nonlinearities in Long Fiber Spans Using a LiNbO3 Phase Conjugator and Raman Amplification, Opitcal Fiber Communication Conference, 2000, vol.4, pp. 266-268, March 2000.

[40] R. H. Stolen, Nonlinearity in Fiber Transmission, Proc. Proc.IEEE, vol. 68, pp. 1232-1236, Oct. 1986.

[41] D. Marcuse, RMS Width of Pulse in Nonlinear Dispersive Fibers, J. Lightwave Technol., vol. 10, pp. 17-21, Jan. 1992.

[42] A. R. Chraplyvy, Limitations on Lightwave Communications Imposed by Optical Fiber Nonlinearities, J. Lightwave Technol., vol. 8, pp. 1548-1557, Oct. 1990.

[43] X. Tang and Z. Wu, Reduction of Intrachannel Nonlinearity Using Optical Phase Conjugation, IEEE Photonics Technol. Lett., vol.17, pp. 1863-1865, Sep. 2005.

[44] R. I. Killey, H. J. Thiele, V. Mikhailov, and P. Bayvel, Reduction of Intrachannel Nonlinear Distortion in 40 Gb/S-based WDM Transmission Over Standard Fiber, IEEE Photonics Technol. Lett., vol.12, pp. 1624-1626, Dec. 2005.

[45] L. Liu, and S. Kumar, Optical Compensation of Fiber Nonlinearities Based on The Theory of Pth-order Inverse, submitted to J. Lightwave Technol.

[46] H. Wei and D. V. Plant, Simultaneous nonlinerity suppression and wide-band dispersion compensation usign optical phase conjugation, Opt. Express, vol.12, pp. 1938-1958, May. 2004.

[47] A. Chowdhury and R. J. Essiambre, Opitcal phase conjugation and pseudolinear transmission, Opt. Lett., vol.29, pp. 1105-1107, May. 2004.

[48] B. Jopson and A. Gnauck, Dispersion Compensation for Optical Fiber Systems, IEEE Communications Magazine, vol.33, pp. 96-102, June 1995.

[49] L. Grüner-Nielsen, M. Wandel, P. Kristensen, C. Jørgensen, L. V. Jørgensen, B. Edvold, B. Pálsdóttir and D. Jakobsen, Dispersion-Compensating Fibers, J. Lightwave Technol., vol.23, pp. 3566-3577, Nov. 2005.

[50] F. Buchali, and H. Bulow, Adaptive PMD Compensation by Electrical and Optical Techniques, J. Lightwave Technol., vol. 22, pp. 1126-1116, April 2004.

[51] C. R. Doerr, S. Chandrasekhar, P. J. Winzer, A. R. Chraplyvy, A. H. Gnauck, L. W. Stulz, R. Pafchek and E. Burrows, J. Lightwave Technol., vol.22, pp. 249-256, Jan. 2004.

[52] K. V. Peddanarappagari and M. Brandt-Pearce, Volterra series transfer function of single-mode fibers, J. Lightwave Technol., vol.15, pp. 2232-2241, Dec.1997.

[53] K. V. Peddanarappagari and M. Brandt-Pearce, Study of fiber nonlinearities in communication systems using a Volterra series transfer function approach, Proc. 31th Annu. Conf. Inform. Sci. Syst., Mar. 1997, pp. 752-757.

[54] B. Xu and M. Brandt-Pearce, Modified Volterra series transfer function Method, IEEE Photonics Technol. Lett., vol.14, pp. 47-49, Jan.2002.

[55] M. Schetzen, Theory of pth-order inverses of nonlinear systems, IEEE Trans. Circuits Syst., vol.cas-23, pp. 285-291, May 1976.

[56] M. Schetzen, Nonlinear system modeling based on the wiener theory, Proceedings of the IEEE, vol.69, pp. 1557-1573, Dec. 1981.

[57] E. Forestieri, Evaluating the Error Probability in Lightwave Systems with Chromatic Dispersion, Arbitrary Pulse Shape and Pre- and Postdetection Filtering, J. Lightwave Technol., vol.18, pp. 1493-1503, Nov.2000.

[58] L. Liu, and S. Kumar, Optical Compensation of Fiber Nonlinearities Based on the Theory of pth-order Inverse, submitted to J. Lightwave Technol.